Molecular Pharmacology Fast Forward. Published on February 8, 2006 as doi:10.1124/mol.105.019802

MOL # 19802

Carboxy-terminal Splicing Enhances Physical Interactions between the Cytoplasmic Tails of Purinergic P2X Receptors

Taka-aki Koshimizu, Karla Kretschmannova, Mu-Lan He, Susumu Ueno, Akito Tanoue, Nobuyuki Yanagihara, Stanko S. Stojilkovic, and Gozoh Tsujimoto

Department of Genomic Drug Discovery Science, Graduate School of Pharmaceutical Sciences Kyoto University Faculty of Pharmaceutical Sciences, Kyoto University, Yoshida Shimoadachi-cho, Sakyo-ku, Kyoto 606-8501, Japan (T.K., G.T.)

Endocrinology and Reproduction Research Branch,
NICHD, National Institutes of Health, Bethesda, Maryland 20892-4510 (K.K., M-L.H., S.S.S.)

Department of Pharmacology,
University of Occupational and Environmental Health, Japan School of Medicine,
Fukuoka 807-8555, Japan (S.U., N.Y.)

Department of Molecular, Cell Pharmacology,
National Research Institute for Child Health and Development, Tokyo 154-3567, Japan (T.K., A.T.)

Molecular Pharmacology Fast Forward. Published on February 8, 2006 as DOI: 10.1124/mol.105.019802
This article has not been copyedited and formatted. The final version may differ from this version.

Running Title: **Interaction between spliced cytoplasmic tails of $P2X_2$**

The number of text pages; 27

Figures; 11

References; 40

Words in the Abstract; 244

Introduction; 532

Discussion; 1324

Address correspondence and reprint requests to:

Gozoh Tsujimoto, M.D., Ph.D.

Department of Genomic Drug Discovery Science, Graduate School of Pharmaceutical Sciences, Kyoto University Faculty of Pharmaceutical Sciences, Kyoto University, Yoshida Shimoadachi-cho, Sakyo-ku, Kyoto 606-8501, Japan

Tel: ++81-75-753-4523, Fax: ++81-75-753-4544, E-mail: gtsuji@pharm.kyoto-u.ac.jp

Abbreviations: BRET, bioluminescent resonance energy transport; $[Ca^{2+}]_i$, intracellular calcium concentration; EST, expressed sequence tag; GFP, green fluorescence protein; GT1 cells, Gonadotropin-releasing hormone-secreting GT1-7 immortalized neurons; HEK cells, human embryonic kidney 293 cells; HEPES, 2-[4-(2-Hydroxyethyl)-1-piperazinyl]ethanesulfonic acid; Luc, luciferase; P2X, ATP-gated receptor-channels; RACE, rapid amplification of cDNA ends; RT-PCR, reverse transcriptase-polymerase chain reaction; YFP, yellow fluorescence protein.

Molecular Pharmacology Fast Forward. Published on February 8, 2006 as DOI: 10.1124/mol.105.019802
This article has not been copyedited and formatted. The final version may differ from this version.

ABSTRACT

Purinergic P2X receptors are ion-conducting channels composed of three subunits, each having two transmembrane domains and intracellular amino (N) and carboxyl (C) termini. Although alternative splicing extensively modifies the C-terminal sequences of P2X subunits, the direct influence of such post-transcriptional modifications on receptor architecture and function remains poorly understood. Here we focused on mouse pituitary $P2X_2$ receptors. In this tissue, progressive splicing of the $P2X_{2a}$ C-terminus generated two functional subunit variants, $P2X_{2b}$ and $P2X_{2e}$, which exhibited accelerated desensitization rates and attenuated calcium signals when the receptors were in homomeric states. To measure the inter-subunit interaction in living cells, the efficient transfer of bioluminescent resonance energy between luciferase and fluorescent proteins attached to the N- or C-subunit termini of these subunits was used. The constitutive interactions between the full-length C-termini of $P2X_{2a}$ receptor were detected by a significant increase in fluorescence/luminescence intensity ratio compared with negative controls. Moreover, interactions between C-termini and between C- and N-termini of adjacent subunits were significantly enhanced in homomeric and heteromeric receptors containing $P2X_{2b}$ or $P2X_{2e}$ subunits. Finally, deletion of two amino acids at the splicing junction, but not at the C-terminal end of the $P2X_{2b}$ receptor, resulted in the enhancement of channel desensitization and luminescence resonance energy transfer. These results indicate that C-terminal structure plays a critical role in the cytoplasmic inter-subunit interactions and suggest that the extent of subunit interactions prior to ATP application could contribute to the subsequent channel activity and conformation changes associated with agonist-dependent desensitization.

Molecular Pharmacology Fast Forward. Published on February 8, 2006 as DOI: 10.1124/mol.105.019802
This article has not been copyedited and formatted. The final version may differ from this version.

INTRODUCTION

P2X receptors, a family of plasma membrane ligand-gated channels, generate a non-selective cationic current in response to activation by extracellular ATP (Ralevic and Burnstock, 1998; Vial et al., 2004). P2X receptors exist as homomeric or heteromeric proteins of three subunits. This architecture has been confirmed by biochemical and mutagenesis studies, as well as by atomic microscopy (Barrera et al., 2005; Jiang et al., 2003; Nicke et al., 1998). Each of the P2X subunits consists of two transmembrane α-helixes connected by a large extracellular loop and intracellular amino (N)- and carboxy (C)-termini (Newbolt et al., 1998; North, 2002; Ralevic and Burnstock, 1998; Torres et al., 1998). Both the N- and C-termini serve as molecular targets for a series of post-transcriptional modifications, including RNA splicing, phosphorylation, and protein-protein interactions with other regulatory molecules (Boue-Grabot et al., 2003; Boue-Grabot et al., 2004; Denlinger et al., 2001; Gendreau et al., 2003; Khakh et al., 2005; Kim et al., 2001; Royle et al., 2002). However, the structural changes introduced into cytoplasmic tails by post-translational modification, particularly in terms of the relationship between the N- and C-termini, were not studied in detail.

In the anterior pituitary, inner ear, and other brain regions, the primary $P2X_2$ gene transcript undergoes extensive alternative splicing resulting in modified mRNA sequences. The spliced subunit termed $P2X_{2b}$ lacks a series of C-terminal 69 amino acids and creates a functional homomeric channel, which desensitizes more rapidly than the full-size receptor, termed $P2X_{2a}$ (Brandle et al., 1997; Koshimizu et al., 1998b; Parker et al., 1998; Simon et al., 1997; Troyanovskaya and Wackym, 1998). Electrostatic charges of six amino acid side chains located close to the proximal splicing site play a critical role in controlling the rate of receptor desensitization (Koshimizu et al., 1999). The C-terminal amino acids of rat $P2X_{2a}$ are also responsible for time- and activation-dependent changes in the permeability induced by channel pore dilation (Eickhorst et al., 2002; Fisher et al., 2004; Khakh et al., 1999; Virginio et al., 1999). On the other hand, phosphorylation of an N-terminal site by protein kinase C significantly accelerates channel desensitization (Boue-Grabot et al., 2000). Although these earlier experiments demonstrate consistent allosteric effects associated with the modification of $P2X_2$ subunit tails leading to changes in channel activity, the possibility of mutual interaction between the N- and C-termini within oligomeric channel architecture was not investigated.

The principal aim of our present study was to directly examine the subunit interactions between N- and C-termini of mouse P2X receptor splicing isoforms in homomeric and

heteromeric configurations and to understand the functional significance of these interactions. To this end, the naturally occurring splicing variants of P2X channels in mouse pituitary were studied by the measurement of bioluminescent resonance energy transfer (BRET) from luciferase (Luc)-tagged C-termini to green florescent protein (GFP)-tagged N- and C-termini. The use of $P2X_{2e}$, which has a shorter C-terminus than $P2X_{2b}$ and desensitizes more rapidly, greatly facilitated our understanding of C-terminal interactions. Our results suggest that heteromeric $P2X_2$ channels are formed by any combination of the three $P2X_2$ splicing subunits found in the pituitary and that conformational constraints generated by splice reactions can enhance energy transfer efficiency and bring the spliced tails in proximity to other subunit tails.

Molecular Pharmacology Fast Forward. Published on February 8, 2006 as DOI: 10.1124/mol.105.019802
This article has not been copyedited and formatted. The final version may differ from this version.

MATERIALS AND METHODS

cDNA Cloning and Expression Analysis of $P2X_2$ Isoforms. The coding sequence of the mouse $P2X_2$ receptor was obtained from pituitary total RNA by RT-PCR. The 5'- and 3'-untranslated regions were obtained by RACE PCR (rapid amplification of cDNA ends) (Clontech, Palo Alto, CA). The primer sequences were designed from the rat $P2X_{2a}$ receptor coding sequence (Brake et al., 1994) and were as follows: 495U (5'-GGACTCCAAGACCTGCGAGGTGT-3') for sense, L1071 (5'-ACAAAATCCAGTCACACAGGAAG-3') for anti-sense, U803 (5'-GGAACTGTGACCTGGACTTG-3') for 3'-RACE, and two anti-sense primers, L598 (5'-TTGGGGTAGTGGATGCTGTTCTT-3') and L43 (5'-TCACCTTGGGCGTCTCGTAGTC-3') for 5'-RACE. Amplified fragments were sub-cloned and at least two independent clones were sequenced using the dideoxy chain termination method and a Megabase 1000 fluorescent sequencer (Amersham Biosciences, Piscataway, NJ). The entire protein-coding regions for the $P2X_2$ subunits were constructed by joining the 5'- and 3'-RACE products.

The tissue distribution of $P2X_2$ splicing isoforms was determined by RT-PCR using a pair of PCR primers that encompass spliced regions: U803 (sense, see earlier for sequence) and L1468 (anti-sense, 5'-CCAGGTCCAGGTCTGTAGCTTA-3'). Amplified PCR products were separated by agarose electrophoresis and then examined by southern blot analysis using an oligonucleotide probe prepared with primer L1008 (5'-TGATGATGGTGGGAATGAGACTGAAT-3'), which is common to all $P2X_2$ isoforms. After hybridization and washing, blots were exposed to image intensifying screens for 12 h and visualized with the aid of a Storm image analyzer (Amersham Biosciences).

Expression of $P2X_2$ Receptors in Mammalian Cells and Current and Intracellular Calcium Measurement. GT1-7 immortalized neurons (GT1 cells) were cultured in Dulbecco's modified Eagle's medium and Ham's F12 medium (1:1). Human embryonic kidney 293 cells (HEK cells) were cultured in Dulbecco's modified Eagle's medium (Invitrogen, Groningen, Netherlands). Both media were supplemented with 10% fetal calf serum, penicillin (50 U/ml) and streptomycin (50 μg/ml). cDNA inserts that had been cloned into the pcDNA3.1 vector (Invitrogen) using *Xho* I and *BamH* I restriction sites were used for transient transfections involving a cationic liposome approach as described previously (Koshimizu et al., 1998a). Single cell $[Ca^{2+}]_i$ recordings were performed 24-48 h after transfection in GT1 cells, as described previously (Koshimizu et al., 1998a). Electrophysiological recordings were done in both GT1 and HEK cells 24-48 hours after

Molecular Pharmacology Fast Forward. Published on February 8, 2006 as DOI: 10.1124/mol.105.019802
This article has not been copyedited and formatted. The final version may differ from this version.

transfection. Cells were continuously perfused with an extracellular solution containing (in mM): 150 NaCl, 3 KCl, 2 $CaCl_2$, 1 $MgCl_2$, 10 2-[4-(2-Hydroxyethyl)-1-piperazinyl]ethanesulfonic acid (HEPES) and 10 glucose. The pH was adjusted to 7.3 with NaOH. Patch pipettes were pulled from borosilicate glass (World Precision Instruments, Sarasota, FL) and heat polished to a tip resistance of 6-7 MW. Pipette solution contained (in mM): 90 K-aspartate, 50 KCl, 3 $MgCl_2$, 10 HEPES and 10 EGTA, adjusted to pH of 7.2 with KOH. Voltage-clamp recordings were performed using Axopatch 200B amplifier (Axon Instruments, Union City, CA). Cells were held at -30 mV throughout recording.

Immunological Detection of $P2X_2$ receptors. PCR was used to insert the FLAG epitope, DYKDDDDK, between the initial methionine residue and the second amino acid of the $P2X_2$ subunit. The 5'-primer was composed of the following sequences: a *Xho*I site (6 bases), an optimized translational sequence (Kozak, 1989), a methionine residue (3 bases), 24 bases encoding the 8-residue FLAG-peptide sequence and 21 bases encoding 7 residues alongside the initial methionine. The 3'-primer for FLAG-tagging was designed between nucleotides 541 to 562 of $P2X_{2a}$. Correctly tagged PCR fragments were transferred to expression constructs using *Xho* I and *Nar* I restriction sites for N-terminal substitutions. Expressed $P2X_2$ constructs were detected with an antibody raised against the $P2X_{2a}$ C-terminus (1:400; Chemicon International Inc., Temecula, CA) or with an anti-FLAG M2 antibody (1:2000; Kodak, Rochester, NY) as described previously (Koshimizu et al., 2002). The secondary antibody used was a peroxidase-conjugated anti-mouse or anti-rat secondary antibody (1:5000, Amersham Biosciences) and signals were visualized by enhanced chemiluminescence ECL (Amersham Biosciences). For immunoprecipitation, 1 μg of antibody was incubated with 1mg cellular lysate (50 mM Tris-HCl, pH = 7.4, 100 mM NaCl, 0.5% NP40, and proteinase inhibitor cocktail, Roche, Basel, Swetzerland) at 4 ˚C for 1 hr and precipitated with protein G sepharose (Amersham Biosciences). Protein concentrations were determined using the Pierce BCA protein assay kit (Pierce, Rockford IL).

Expression in *Xenopus Laevis* Oocytes and Electrophysiological Recordings. Oocytes (at developmental stages V and VI) were isolated from adult *X. laevis* as described previously (Beckstead et al., 2000) and placed in modified Barth's saline containing: 88 mM NaCl, 1 mM KCl, 10 mM HEPES, 0.82 mM $MgSO_4$, 2.4 mM $NaHCO_3$, 0.91 mM $CaCl_2$, and 0.33 mM $Ca(NO_3)_2$ at pH 7.5. The oocyte nuclei were injected directly with 0.5 ng of each expression construct ($P2X_{2a}$, $P2X_{2b}$, or $P2X_{2e}$) in 30 nl of injection buffer (88 mM NaCl, 1 mM KCl, 15 mM HEPES, at pH 7.0).

Molecular Pharmacology Fast Forward. Published on February 8, 2006 as DOI: 10.1124/mol.105.019802
This article has not been copyedited and formatted. The final version may differ from this version.

Injected oocytes were maintained for two days at 18 ˚C in sterile incubation medium containing modified Barth's saline plus 10 μg/ml streptomycin, 10 units/ml penicillin, 50 μg/ml gentamicin and 2 mM sodium pyruvate. For electrophysiological recording, oocytes were placed in a rectangular chamber (100 μl volume) and perfused with Ba^{2+}-Ringer's solution (in mM: 115 NaCl, 2.5 KCl, 1.8 $BaCl_2$, and 10 HEPES, pH 7.4) at a rate of 2 ml/min. The oocytes were then impaled with two glass electrodes (0.5-10 MΩ) pre-filled with 3 M KCl and were subsequently voltage-clamped at -50 mV using an OC-725C Oocyte Clamp Amplifier (Warner Instruments, Inc., Hamden, CT). Currents were digitally recorded with a PowerLab/200 system along with Chart software (ADInstruments, Grand Junction, CO). ATP was dissolved in distilled water and then diluted in Ba^{2+}-Ringer's solution immediately before use and applied for 30 s. All measurements were performed at ambient temperature.

Construction of Mutant Subunits. Mutant $P2X_2$ subunits were created by PCR methodology. For the N-terminally deleted $P2X_2$ subunits, which lack the first 13 amino acids but retain the second AUG codon, PCR primers U1 (5'-GGCCGTGTGGGGTGTTCATCTCT-3') and L1468 (see earlier for sequence) were used. The primer used to delete two amino acids at the distal end of the $P2X_{2b}$ subunits was 5'-GGTACCGGCCAAACCTTTGGGGTCCGTGGATGTGG-3'. Two further amino acids were removed at the proximal splicing junction using two overlapping primers: 5'-GGTCAAGAGTGTCCTTGTCGAACTTCTTATGG-3' and 5'-AAGTTCGACAAGGACACTCTTGACCAGCATATGGGAC-3'. The PCR products were sub-cloned, sequenced and the verified inserts subsequently directionally cloned into the pcDNA vector using *Xho* I and *BamH* I restriction sites.

BRET Assay. The cDNAs encoding each of the P2X receptors were fused in-frame with the coding sequences for either yellow fluorescent protein (YFP) or Renilla luciferase gene (Luc; Promega) by changing the native stop codon to a *Kpn*I restriction enzyme site, resulting in two amino acid insertions of glycine and asparagine between the receptor and either YFP or Luc. For YFP, a brighter variant, Venus (F64L/M153T/V163A/S175G) (Nagai et al., 2002), was used. All fusion constructs were sequenced and subsequently cloned into the pcDNA3.1 vector (Invitrogen). For Luc-connected $P2X_2$ subunit, N-terminal FLAG epitope was inserted as described above. Expression of GFP- and YFP-fusion receptors were confirmed by monoclonal anti-GFP antibody (1:2000, MBL, Tokyo, Japan).

For BRET assays, transfected cells were grown on a 10-cm culture dish, collected in PBS containing 1mM EDTA and then suspended in Hank's/HEPES buffer at a concentration of 1 x

Molecular Pharmacology Fast Forward. Published on February 8, 2006 as DOI: 10.1124/mol.105.019802
This article has not been copyedited and formatted. The final version may differ from this version.

10^6/ml. Luminescence spectra were measured by a fluorescence spectrophotometer (F-4500, Hitachi, Tokyo, Japan) after the addition of coelenterazine h (Promega) at a final concentration of 5 μM. The BRET signal was then determined by calculating the signal ratio of the light emitted by the receptor-YFP fusion at 535 nm or the receptor-GFP fusion at 515 nm to the light emitted by the receptor-Luc fusion at 480 nm. The background signal was determined prior to the addition of coelenterazine h and was subtracted from experimental values. The background signal intensity was always less than 1% of the measured values. Steady-state fluorescence anisotropy was measured in a suspension of cells at a concentration of 10^5/ml expressing single receptors expressing fluorescent protein tags receptors. This procedure was performed in assay buffer containing 137 mM NaCl, 5 mM KCl, 1.2 mM $CaCl_2$, 1 mM $MgCl_2$, 10 mM HEPES, and 10 mM glucose using a computer-controlled and thermostatically-regulated spectrophotofluorimeter (MPF-2A, Hitachi, Tokyo, Japan).

Calculations. All data are represented as mean ± SEM values. Significant differences, with $P < 0.05$, were determined by One-way ANOVA followed by Newman-Keuls multiple comparison test. Concentration-response relationships were fitted to a four-parameter logistic equation using a non-linear curve-fitting program, from which the EC_{50} and Hill's values were derived (Kaleidagraph, Synergy Software, Reading, PA). The declining phases of the observed calcium responses were fitted to single-exponential functions (GraphPad Prism, GraphPad Software, San Diego, CA) and results were assessed according to the "extra sum of squares" principle, as described previously (Koshimizu et al., 2002).

Molecular Pharmacology Fast Forward. Published on February 8, 2006 as DOI: 10.1124/mol.105.019802
This article has not been copyedited and formatted. The final version may differ from this version.

RESULTS

Splicing Variants of $P2X_2$ Subunit in Mouse Pituitary. In the anterior pituitary tissue of mice, we identified three C-terminal splicing variants, termed $P2X_{2a}$, $P2X_{2b}$ and $P2X_{2e}$ (Fig. 1A). The $P2X_{2b}$ subunit lost a stretch of 69 amino acids in keeping with the original reading flame and C-terminal end, which is entirely consistent with prior literature (Brandle et al., 1997; Housley et al., 1999; Koshimizu et al., 1998b; Simon et al., 1997; Troyanovskaya and Wackym, 1998). In $P2X_{2e}$ subtype, 90 amino acids are deleted from the C-terminus (from Val^{383} to Glu^{472}) and the C-terminal end was preserved (Fig. 1A). A splicing pattern similar to the pituitary $P2X_{2e}$ was previously reported as a partial transcript isolated from rat vestibular end-organs, but the functional properties of this subunit were not investigated (Troyanovskaya and Wackym, 1998). In contrast to rat $P2X_2$ subunits, the cytoplasmic N-terminus of three mouse $P2X_2$ subunits contained additional 13 amino acids. RT-PCR analysis revealed that the $P2X_{2a}$ subunit was the most abundant transcript and was detected in a variety of tissues, whilst the $P2X_{2e}$ subunit was detected only in the pituitary (Fig. 1B and 1C). When $P2X_2$ subunits were separately expressed in HEK (Fig. 1D) and GT1 cells (not shown), the differences in molecular weight between spliced and full-length $P2X_2$ variants were immunologically detected by western blot analysis. Relatively broad bands seen on the blot indicate the glycosylated mature subunits. In cells expressing $P2X_{2a}$, no additional lower band corresponding to the spliced $P2X_{2b}$ or $P2X_{2e}$ was detected, suggesting that further splicing reaction on the full-length C-terminus did not occur in these cells.

Signaling Patterns by Native and Mutant Receptors. We expressed these subunits in mammalian GT1 and HEK cells, as well as in *Xenopus* oocytes, to evaluate the impact of different C-terminal splicing patterns on channel function. When expressed as homomeric channels in GT1 and HEK cells, the full-length and two spliced $P2X_2$ receptors were functional, as indicated by generation of high amplitude inward currents in response to 100 μM ATP application (Fig. 2). However, channels generated different pattern of currents during the prolonged application of ATP. $P2X_{2a}$ receptor desensitized with the time constants (τ_{des}) of about 10 s and 12 s in GT1 and HEK cells, respectively (Fig. 2A). In both cell types, $P2X_{2b}$ desensitized more rapidly, with the time constants of about 5 s (Fig. 2B). The additional reduction in C-terminal sequence in $P2X_{2e}$ spliced form resulted in a channel that desensitized with τ_{des} between 0.5 s and 0.7 s, the rates highly comparable to the rapidly desensitizing $P2X_1$ and $P2X_3$ receptors (Fig. 2C).

Experiments with single cell calcium measurements were done only in GT1 cells, because HEK cells express calcium-mobilizing P2Y receptors (He et al., 2003). All three channels

Molecular Pharmacology Fast Forward. Published on February 8, 2006 as DOI: 10.1124/mol.105.019802
This article has not been copyedited and formatted. The final version may differ from this version.

responded to application of ATP with rapid and concentration-dependent increases in $[Ca^{2+}]_i$, exhibiting comparable EC_{50} values (10, 4, and 12 μM, for $P2X_{2a}$, $P2X_{2b}$, and $P2X_{2e}$, respectively; n = 8-14). However, in all ATP doses applied the peak amplitude of $[Ca^{2+}]_i$ signals in $P2X_{2e}$-expressing cells were significantly lower compared with responses observed in $P2X_{2a}$ and $P2X_{2b}$-expressing cells (Fig. 3). The desensitizing rates of ATP-induced $[Ca^{2+}]_i$ signals were also dependent on ATP concentration; the calculated EC_{50} values for $[Ca^{2+}]_i$ decay rate were 25 μM, 50 μM and 16 μM for $P2X_{2a}$, $P2X_{2b}$, and $P2X_{2e}$, respectively (n = 7-12). As in current measurements (Fig. 2), the three channels differed in the decay rates of $[Ca^{2+}]_i$ after peak values when stimulated with 100 μM ATP (Fig. 3). We also found that there were significant differences in plateau $[Ca^{2+}]_i$ values among the three isoforms. Five minutes after the peak increase, the reductions in $[Ca^{2+}]_i$ were 62.3 ± 2 %, 83.7 ± 1.4 %, and 94.5 ± 0.6 %, for $P2X_{2a}$, $P2X_{2b}$ and $P2X_{2e}$, respectively.

Consistent with single cell current and calcium measurements in mammalian cells, the electrophysiological examination of the three splicing variants expressed in *Xenopus* oocytes revealed differences in the rates of receptor desensitization in response to supra-maximal (100 μM) concentrations of agonist (Fig. 4B and C). However, the rates of current decay in the presence of agonists were slower for all three receptors, compared with the rates observed in mammalian cells, indicating the cell-type specificity in the expression of $P2X_2$ receptors. Differences in current kinetics were observed for $P2X_4$ receptor, when the receptor was expressed in mammalian cells and *Xenopus* oocytes (North, 2002).

To examine the relevance of 13 N-terminal residues of mouse $P2X_2$, which are not present in rat receptors, on channel activity, we generated three mutants by deleting these residues (termed $P2X_{2a}\Delta 1\text{-}13$, $P2X_{2b}\Delta 1\text{-}13$, and $P2X_{2e}\Delta 1\text{-}13$; Fig. 4A) and expressed them in *Xenopus* oocytes and GT1 cells. As shown in Fig. 4B and C, N-terminal deletion introduced together with progressive splicing at the C-termini had additive effects on accelerating rates of receptor desensitization. The combined effects of C- and N-terminal deletion on single cell $[Ca^{2+}]_i$ profiles was also evident in $[Ca^{2+}]_i$ measurements in GT1 cells expressing $P2X_{2a}$ and $P2X_{2b}$ wild type and mutant receptors (Fig. 5). In the case of $P2X_{2e}$ and $P2X_{2e}\Delta 1\text{-}13$, $[Ca^{2+}]_i$ kinetics were comparable, probably reflecting the resolution limit in these measurements. We also found that deletion at the N-terminus did not affect steady $[Ca^{2+}]_i$ levels five minutes after the peak increase (Fig. 5). Finally, the EC_{50} values of the N-terminal deletion mutants were not significantly altered when compared to values for $P2X_{2a}$ (12, 7, and 8 μM, for $P2X_{2a}\Delta 1\text{-}13$, $P2X_{2b}\Delta 1\text{-}13$, and $P2X_{2e}\Delta 1\text{-}13$, respectively). Therefore, the deletion of N-terminal ends of mouse $P2X_2$ subunits accelerates receptor

Molecular Pharmacology Fast Forward. Published on February 8, 2006 as DOI: 10.1124/mol.105.019802
This article has not been copyedited and formatted. The final version may differ from this version.

desensitization, and this N-terminal deletion and the C-terminal splicing have an additive effect on the rates of receptor desensitization.

Detection of Inter-subunit Interactions Between Cytoplasmic Tails by BRET. To visualize protein-protein interactions between the cytoplasmic tails of channel-forming subunits, we measured the bioluminescent resonance energy transfer from Luc tagged at the C-terminus subunit to GFP tagged to the N-terminus, or to YFP tagged to the C-terminus. The addition of Luc or fluorescent proteins to any of the $P2X_2$ subunit constructs described here caused no detectable changes in the pattern of receptor expression at the plasma membrane or alteration in the channel function in terms of EC_{50} value, peak $[Ca^{2+}]_i$ response to ATP, or the rate of calcium signal decay. Figure 6A illustrates the dose-dependence of ATP-induced $[Ca^{2+}]_i$ responses for $P2X_{2a}$-YFP and $P2X_{2a}$-Luc constructs, with the EC_{50} values highly comparable to the non-tagged receptors (Fig. 3). Figure 6B, top shows the plasma membrane localization of the receptors with YFP tagged at C-termini, whereas Fig. 6B, bottom illustrates the profiles of Ca^{2+} signals in GT1 cells expressing these constructs. These results clearly indicate that the subunit-specific Ca^{2+} signals are preserved after C-terminal modifications.

In addition, no difference was observed in steady-state anisotropy measurements of cells expressing the GFP- or YFP-tagged receptors (data not shown). We also confirmed the expression of tagged subunit proteins on the western blot membrane (Fig. 6C). Furthermore, differently tagged subunits were co-immunoprecipitated (Fig. 6D). The accelerated rates of receptor desensitization for the spliced isoforms were preserved after N- and C-terminal tagging (Fig. 6E). Finally, the heteromer-specific channel response was detected by co-expressing YFP-tagged $P2X_{2a}$ or $P2X_{2e}$ subunits with chimeric $P2X_{2a}/X_3$ex, in which the extracellular domain of $P2X_{2a}$ was replaced with that of $P2X_3$ (Koshimizu et al., 2002). As shown in Fig. 6F, both heteromeric channels responded to 10 μM αβ-methylene ATP application with a rise in $[Ca^{2+}]_i$, but the faster decay of $[Ca^{2+}]_i$ was seen in cells expressing YFP-tagged $P2X_{2e}$ + $P2X_{2a}/X_3$ex. None of native $P2X_2$ subunits made homomeric channels responsive to 10 μM αβ-methylene ATP (Koshimizu et al., 2002, and data not shown for YFP-tagged $P2X_{2a}$ or $P2X_{2e}$). Therefore, tagged $P2X_2$ subunits retained the ability to form functional homomeric and heteromeric channels without affecting the protein expression, trafficking, and functionalities of P2X subunits.

We then titrated the expression levels of the $P2X_2$-Luc and $P2X_2$-YFP constructs similar to those expressing Luc and YFP alone. When $P2X_{2a}$-Luc and $P2X_{2a}$-YFP were co-expressed,

Molecular Pharmacology Fast Forward. Published on February 8, 2006 as DOI: 10.1124/mol.105.019802
This article has not been copyedited and formatted. The final version may differ from this version.

subunit oligomerization was specifically detected by BRET, which occurred from the C-terminally tagged Luc to YFP (Fig. 7A). The signal intensity ratio at 535 nm/480 nm was significantly higher in cells expressing $P2X_{2a}$-Luc and $P2X_{2a}$-YFP (0.52 ± 0.02 n=10) than those of control cells expressing Luc and $P2X_{2a}$-YFP (0.38 ± 0.03, n=4) or $P2X_{2a}$-Luc and YFP (0.35 ± 0.03, n=4). In contrast, the co-expression of the α_{1b}-adrenergic receptor, a G-protein-coupled plasma membrane receptor with heptahelical membrane topology, together with the $P2X_{2a}$ subunit did not induce significant change in BRET value (Fig. 7A). The protein expression levels (Fig. 7B) or stimulations with 100 μM ATP (Fig. 7C) did not alter BRET signals in mouse $P2X_2$ receptors.

Inter-subunit interactions of the cytoplasmic tails were detected by BRET analysis in any combination of full-length or spliced $P2X_2$ subunits. Moreover, shortening the C-termini by progressive splicing resulted in accelerated energy transfer efficiency, as shown in Fig. 8. Specifically, the BRET signal of homomeric $P2X_{2e}$ receptors was significantly stronger than that of control construct Luc-YFP, in which Luc and YFP were fused directly by a spacer consisting of two amino acids (Gly-Thy); BRET signals were 1.03 ± 0.02 and 0.94 ± 0.01 for $P2X_{2e}$ and the Luc-YFP construct, respectively (n = 5). Furthermore, interactions between the C- and N-termini of adjacent subunits were detected as the BRET signal and C-terminal splicing significantly increased the BRET efficiency (Fig. 9). These results indicate that C-terminal splicing enhances the inter-subunit interactions between the C-termini and the N- and C-terminal ends of $P2X_2$ receptors.

The splicing pattern-dependent conformational changes were not due to the shortening of the C-terminal, because the consequence of C-terminal mutation was sequence-specific. For example, deletion of two amino acids at the splicing junction of $P2X_{2b}$, where channel function had been altered in previous mutagenesis studies, resulted in an increase in BRET efficiency, while mutation at the C-terminus had no effect (Fig. 10A and 10B). When these $P2X_{2b}$ receptor mutants were examined functionally, the desensitization rate of $P2X_{2b}\Delta 370\text{-}371$ was significantly faster than those of $P2X_{2b}$ and $P2X_{2b}\Delta 402\text{-}403$ (Fig. 10C). These results indicate that removal of a critical C-terminal amino acid stretch could have a sequence-specific effect on both the subunit interaction and the channel activity.

To examine whether increased BRET at cytoplasmic tails corresponds to tight subunit assembly in $P2X_{2e}$ channels, $P2X_{2a}$-YFP or $P2X_{2e}$-YFP was co-immunoprecipitated with Flag-$P2X_{2a}$-Luc using anti-Flag antibody, and the immunocomplexes were washed with

Molecular Pharmacology Fast Forward. Published on February 8, 2006 as DOI: 10.1124/mol.105.019802
This article has not been copyedited and formatted. The final version may differ from this version.

increasing concentrations of detergent (Fig. 11). This treatment removed part of $P2X_{2e}$-YFP bond to Flag-$P2X_{2a}$-Luc, but not $P2X_{2a}$-YFP (Fig. 11). Thus, the inter-subunit interactions at C-termini, which can be detected by BRET, do not necessarily correlate with biochemical tightness of subunit assembly.

Molecular Pharmacology Fast Forward. Published on February 8, 2006 as DOI: 10.1124/mol.105.019802
This article has not been copyedited and formatted. The final version may differ from this version.

DISCUSSION

In this study, we analyzed the expression of $P2X_2$ receptors in mouse pituitary cells and the functional significance of inter-subunit interactions occurring at the receptor N- and C-termini was evaluated by measuring current and calcium signaling. Our results indicate that mouse pituitary express three forms of $P2X_2$ receptors, the full size $P2X_{2a}$ and the spliced forms $P2X_{2b}$ and $P2X_{2e}$ missing 69 and 90 residues in their C-termini, respectively. When compared with rat pituitary $P2X_2$ receptors, all three mouse forms have additional 13 N-terminal residues. Analysis of exon-intron boundaries in the mouse $P2X_2$ gene by both molecular cloning and sequence database searches indicated that the $P2X_2$ gene is composed of eleven exons and that the last exon contains the entire cytoplasmic C-tail and half of the second transmembrane domain. To generate C-terminal splicing variants in the pituitary, it is necessary to use cryptic splicing donor/acceptor sites in the last exon. Although such tissue-specific splicing machinery acting upon the primary $P2X_2$ transcript needs to be examined more closely, the forced expression of $P2X_{2a}$ in either neuronal GT1 cells or kidney HEK cell did not produce shorter subunits, enabling us to analyze the splicing pattern-specific function.

Among the $P2X_2$ isoforms examined here and in the previous reports (Chen and Bobbin, 1998; Housley et al., 1995; Koshimizu et al., 1998b; Parker et al., 1998; Simon et al., 1997; Troyanovskaya and Wackym, 1998), $P2X_{2e}$ exhibited the fastest desensitization rate, as estimated by current measurements. The fast desensitization rate of mouse $P2X_{2e}$ receptor found in this study was apparently comparable to the rates of rapidly desensitizing $P2X_1$ and $P2X_3$ receptors reported previously (North, 2002), whereas the EC_{50} for ATP for this receptor was comparable to the full size $P2X_{2a}$ receptor. The rate of $P2X_{2b}$ receptor desensitization was faster than $P2X_{2a}$ but slower than $P2X_{2e}$ receptors and comparable to rates of $P2X_4$ receptor desensitization. These C-terminal deletions in turn effectively reduced the peak amplitude and duration of calcium signals. Finally, $P2X_{2e}$ spliced form was specific for pituitary tissue. Because the ion-permeating pores of P2X receptors are formed by three subunits (Barrera et al., 2005; Jiang et al., 2003; Nicke et al., 1998) and three splicing variants could be derived from the same primary $P2X_2$ transcript, it is probable that a single pituitary cell expresses a series of homo- and heteromeric $P2X_2$ channels.

The present results suggest that the amino acid length of the $P2X_2$ C-terminus is not a primary determinant of C-terminus-dependent channel desensitization, because the deletion of two amino acids at the splicing acceptor site, but not at the distal C-terminal end, resulted in accelerated rates of desensitization. Previous studies of the C-terminus-dependent desensitization

Molecular Pharmacology Fast Forward. Published on February 8, 2006 as DOI: 10.1124/mol.105.019802
This article has not been copyedited and formatted. The final version may differ from this version.

of rat $P2X_2$ (Koshimizu et al., 1999; Smith et al., 1999) also showed that mutants possessing shorter C-termini than that of $P2X_{2e}$ retained the full channel activity, and that two candidate amino acid regions were critical for C-terminus-dependent desensitization: the Val^{383} residue and the negative static charges of the adjacent six amino acids located at the splicing donor site (Koshimizu et al., 1999; Smith et al., 1999). These residues were absent in the $P2X_{2e}$ C-terminus, possibly explaining the accelerated desensitization rate associated with $P2X_{2e}$. These results may indicate that $P2X_{2b}$ and $P2X_{2e}$ serve as a dominant negative tool to limit duration of signaling and cellular responsiveness by homo- and heteromeric $P2X_2$ receptors, such as $P2X_2/P2X_3$ receptors in sensory pathways and other purinergic systems (Ralevic and Burnstock, 1998).

The structure of the N-terminal tail also influences the duration of $P2X_2$-mediated channel signaling in the continuous presence of an agonist. Species-specific differences were found when comparing the desensitization rates of human and rat $P2X_{2b}$ subunits; unlike rat $P2X_{2b}$, human $P2X_{2b}$ desensitized at a rate similar to human $P2X_{2a}$ (Lynch et al., 1999). The main structural distinction between human and rat $P2X_{2b}$ subunits is at the N-termini, in which the human orthologue has an additional 13 amino acids. However, our data suggested that this difference in sequence does not explain the observed species-specific difference in activity, because deletion of the first 13 amino acids at the N-terminus of mouse $P2X_2$ resulted in accelerated desensitization rates of all C-terminal splicing isoforms. Instead, we found that the combined effect of shortening both the cytoplasmic N- and C-terminal ends on overall channel function of mouse $P2X_2$ was additive, accelerating the desensitization rates.

We also explored the presence and functional significance of inter-subunit interactions at the N- and C-termini of pituitary $P2X_2$ receptor subunits in living cells. Our results indicate that $P2X_2$ receptors connected to GFP/YFP or Luc were fully functional, and the N- and C-terminal interactions were possible among all $P2X_2$ subunit combinations. Patch clump analysis from open channel lifetimes, open channel noise and kinetics indicate that the $P2X_{2a}$ receptors are not independent, but have positive cooperativity (Ding and Sachs, 2002). Thus, it might be possible that subunit interactions could occur, in part, between cytoplasmic tails of clustered $P2X_2$ channels. The efficiency of energy transfer changes in accordance with the distance and the relative orientation of energy donor and acceptor pair. Steady-state fluorescence anisotropy measurements revealed that there were no significant differences amongst the $P2X_2$ constructs investigated here, suggesting that C-terminal splicing resulted in reductions of relative C-terminal distance and increased inter-subunit interaction. In line with our previous study reporting that heteromers

Molecular Pharmacology Fast Forward. Published on February 8, 2006 as DOI: 10.1124/mol.105.019802
This article has not been copyedited and formatted. The final version may differ from this version.

composed of full-length and spliced C-termini of rat $P2X_2$ desensitized faster than $P2X_{2a}$ homomers but slower than $P2X_{2b}$ homomers (Koshimizu et al., 2002), we also show here that heteromultimer formation with $P2X_{2e}$-YFP and $P2X_{2a}$/X3ex resulted in an acceleration in desensitization rate, compared to that of channels formed by $P2X_{2a}$-YFP and $P2X_{2a}$/X3ex. These results indicate that there is a consistent parallelism between the level of constitutive inter-subunit interactions and the rates of receptor desensitization. Furthermore, inter-subunit interactions at the spliced C-termini increased BRET signals in both homomeric and heteromeric channels.

A recent study revealed that differences at the distal C-terminal tail structure of rat and mouse $P2X_{2a}$ expressed in *Xenopus* oocytes account for a transition in pore permeability, from sodium selective to organic cation permeable, which is seen in rat $P2X_{2a}$ but not in mouse homologues (Eickhorst et al., 2002). In addition, FRET signals detected by total reflection microscopy decrease during the prolonged activation of rat $P2X_{2a}$ receptors expressed in HEK cells with a time course similar to pore dilatation. The wild type and mutant channels that did not undergo permeability changes also did not show evidence of cytosolic gating motions (Fisher et al., 2004). In full agreement with these results, we found that BRET signals were not altered after stimulation of mouse $P2X_{2a}$ with ATP and that C-terminal splicing variants had constitutive inter-subunit interactions. These results suggest that the strength of mutual interactions at the $P2X_2$ C-terminus positively correlates with BRET/FRET efficiency and negatively correlates with the signal length by $P2X_2$ receptors during continuous or repetitive agonist applications. The relationship between inter-subunit interaction and function of the other ligand-gated channel was also reported recently; in the AMPA type glutamate receptor an increase in the likelihood of subunit interaction at the ligand-binding domain results in decreased receptor desensitization (Sun et al., 2002). Thus, analyzing inter-subunit interactions in relation to receptor activity could further advance our understanding of conformational constraint and transitions of the ligand-gated channel molecule.

In conclusion, our results demonstrated the critical contribution of spliced C-tails in the formation of functional channel through subunit interaction. Shortening the subunit C-terminus and deleting the N-termini had an additive effect on the desensitization rates of $P2X_2$ receptors. The distinct desensitization patterns caused by C-terminal splicing were preserved even after N-terminal deletions. Moreover, diverse heteromeric $P2X_2$ channels are formed in any combination of the three $P2X_2$ splicing subunits found in the pituitary. The rates of receptor desensitization of these homo- and heteromeric channels positively correlated to the energy

Molecular Pharmacology Fast Forward. Published on February 8, 2006 as DOI: 10.1124/mol.105.019802
This article has not been copyedited and formatted. The final version may differ from this version.

transfer efficiency between tagged subunits. These results suggest that the extent of $P2X_2$ subunit interactions at cytoplasmic tails in the absence of ATP could play a key role in shaping the ATP-dependent opening of channels and calcium signaling in pituitary and other cell types.

Molecular Pharmacology Fast Forward. Published on February 8, 2006 as DOI: 10.1124/mol.105.019802
This article has not been copyedited and formatted. The final version may differ from this version.

REFERENCES

Barrera NP, Ormond SJ, Henderson RM, Murrell-Lagnado RD and Edwardson JM (2005) Atomic force microscopy imaging demonstrates that P2X2 receptors are trimers but that P2X6 receptor subunits do not oligomerize. *J Biol Chem* **280**:10759-65.

Beckstead MJ, Weiner JL, Eger EI, 2nd, Gong DH and Mihic SJ (2000) Glycine and gamma-aminobutyric acid(A) receptor function is enhanced by inhaled drugs of abuse. *Mol Pharmacol* **57**:1199-205.

Boue-Grabot E, Archambault V and Seguela P (2000) A protein kinase C site highly conserved in P2X subunits controls the desensitization kinetics of P2X(2) ATP-gated channels. *J Biol Chem* **275**:10190-5.

Boue-Grabot E, Barajas-Lopez C, Chakfe Y, Blais D, Belanger D, Emerit MB and Seguela P (2003) Intracellular cross talk and physical interaction between two classes of neurotransmitter-gated channels. *J Neurosci* **23**:1246-53.

Boue-Grabot E, Emerit MB, Toulme E, Seguela P and Garret M (2004) Cross-talk and co-trafficking between rho1/GABA receptors and ATP-gated channels. *J Biol Chem* **279**:6967-75. Epub 2003 Dec 1.

Brake AJ, Wagenbach MJ and Julius D (1994) New structural motif for ligand-gated ion channels defined by an ionotropic ATP receptor. *Nature* **371**:519-23.

Brandle U, Spielmanns P, Osteroth R, Sim J, Surprenant A, Buell G, Ruppersberg JP, Plinkert PK, Zenner HP and Glowatzki E (1997) Desensitization of the P2X(2) receptor controlled by alternative splicing. *FEBS Lett* **404**:294-8.

Chen C and Bobbin RP (1998) P2X receptors in cochlear Deiters' cells. *Br J Pharmacol* **124**:337-44.

Denlinger LC, Fisette PL, Sommer JA, Watters JJ, Prabhu U, Dubyak GR, Proctor RA and Bertics PJ (2001) Cutting edge: the nucleotide receptor P2X7 contains multiple protein- and lipid-interaction motifs including a potential binding site for bacterial lipopolysaccharide. *J Immunol* **167**:1871-6.

Ding S and Sachs F (2002) Evidence for non-independent gating of P2X2 receptors expressed in Xenopus oocytes. *BMC Neurosci* **3**:17.

Eickhorst AN, Berson A, Cockayne D, Lester HA and Khakh BS (2002) Control of P2X(2)

channel permeability by the cytosolic domain. *J Gen Physiol* **120**:119-31.

Fisher JA, Girdler G and Khakh BS (2004) Time-resolved measurement of state-specific P2X2 ion channel cytosolic gating motions. *J Neurosci* **24**:10475-87.

Gendreau S, Schirmer J and Schmalzing G (2003) Identification of a tubulin binding motif on the P2X(2) receptor. *J Chromatogr B Analyt Technol Biomed Life Sci* **786**:311-8.

He ML, Zemkova H, Koshimizu T, Tomic M and Stojilkovic SS (2003) Intracellular calcium measurements as a method in studies on activity of purinergic P2X receptor channels. *Am J Physiol Cell Physiol* **285**:C467-79. Epub 2003 Apr 23.

Housley GD, Greenwood D, Bennett T and Ryan AF (1995) Identification of a short form of the P2xR1-purinoceptor subunit produced by alternative splicing in the pituitary and cochlea. *Biochem Biophys Res Commun* **212**:501-8.

Housley GD, Kanjhan R, Raybould NP, Greenwood D, Salih SG, Jarlebark L, Burton LD, Setz VC, Cannell MB, Soeller C, Christie DL, Usami S, Matsubara A, Yoshie H, Ryan AF and Thorne PR (1999) Expression of the P2X(2) receptor subunit of the ATP-gated ion channel in the cochlea: implications for sound transduction and auditory neurotransmission. *J Neurosci* **19**:8377-88.

Jiang LH, Kim M, Spelta V, Bo X, Surprenant A and North RA (2003) Subunit arrangement in P2X receptors. *J Neurosci* **23**:8903-10.

Khakh BS, Bao XR, Labarca C and Lester HA (1999) Neuronal P2X transmitter-gated cation channels change their ion selectivity in seconds. *Nat Neurosci* **2**:322-30.

Khakh BS, Fisher JA, Nashmi R, Bowser DN and Lester HA (2005) An angstrom scale interaction between plasma membrane ATP-gated P2X2 and alpha4beta2 nicotinic channels measured with fluorescence resonance energy transfer and total internal reflection fluorescence microscopy. *J Neurosci* **25**:6911-20.

Kim M, Jiang LH, Wilson HL, North RA and Surprenant A (2001) Proteomic and functional evidence for a P2X7 receptor signalling complex. *Embo J* **20**:6347-58.

Koshimizu T, Koshimizu M and Stojilkovic SS (1999) Contributions of the C-terminal domain to the control of P2X receptor desensitization. *J Biol Chem* **274**:37651-7.

Koshimizu T, Tomic M, Koshimizu M and Stojilkovic SS (1998a) Identification of amino acid residues contributing to desensitization of the P2X2 receptor channel. *J Biol Chem* **273**:12853-7.

Koshimizu T, Tomic M, Van Goor F and Stojilkovic SS (1998b) Functional role of alternative

splicing in pituitary P2X2 receptor- channel activation and desensitization. *Mol Endocrinol* **12**:901-13.

Koshimizu T, Ueno S, Tanoue A, Yanagihara N, Stojilkovic SS and Tsujimoto G (2002) Heteromultimerization modulates P2X receptor functions through participating extracellular and C-terminal subdomains. *J Biol Chem* **277**:46891-9.

Kozak M (1989) The scanning model for translation: an update. *J Cell Biol* **108**:229-41.

Lynch KJ, Touma E, Niforatos W, Kage KL, Burgard EC, van Biesen T, Kowaluk EA and Jarvis MF (1999) Molecular and functional characterization of human P2X(2) receptors. *Mol Pharmacol* **56**:1171-81.

Nagai T, Ibata K, Park ES, Kubota M, Mikoshiba K and Miyawaki A (2002) A variant of yellow fluorescent protein with fast and efficient maturation for cell-biological applications. *Nat Biotechnol* **20**:87-90.

Newbolt A, Stoop R, Virginio C, Surprenant A, North RA, Buell G and Rassendren F (1998) Membrane topology of an ATP-gated ion channel (P2X receptor). *J Biol Chem* **273**:15177-82.

Nicke A, Baumert HG, Rettinger J, Eichele A, Lambrecht G, Mutschler E and Schmalzing G (1998) P2X1 and P2X3 receptors form stable trimers: a novel structural motif of ligand-gated ion channels. *Embo J* **17**:3016-28.

North RA (2002) Molecular physiology of P2X receptors. *Physiol Rev* **82**:1013-67.

Parker MS, Larroque ML, Campbell JM, Bobbin RP and Deininger PL (1998) Novel variant of the P2X2 ATP receptor from the guinea pig organ of Corti. *Hear Res* **121**:62-70.

Ralevic V and Burnstock G (1998) Receptors for purines and pyrimidines. *Pharmacol Rev* **50**:413-92.

Royle SJ, Bobanovic LK and Murrell-Lagnado RD (2002) Identification of a non-canonical tyrosine-based endocytic motif in an ionotropic receptor. *J Biol Chem* **277**:35378-85.

Simon J, Kidd EJ, Smith FM, Chessell IP, Murrell-Lagnado R, Humphrey PP and Barnard EA (1997) Localization and functional expression of splice variants of the P2X2 receptor. *Mol Pharmacol* **52**:237-48.

Smith FM, Humphrey PP and Murrell-Lagnado RD (1999) Identification of amino acids within the P2X2 receptor C-terminus that regulate desensitization. *J Physiol* **520 Pt 1**:91-9.

Sun Y, Olson R, Horning M, Armstrong N, Mayer M and Gouaux E (2002) Mechanism of glutamate receptor desensitization. *Nature* **417**:245-53.

Torres GE, Egan TM and Voigt MM (1998) Topological analysis of the ATP-gated ionotropic P2X2 receptor subunit. *FEBS Lett* **425**:19-23.

Troyanovskaya M and Wackym PA (1998) Evidence for three additional P2X2 purinoceptor isoforms produced by alternative splicing in the adult rat vestibular end-organs. *Hear Res* **126**:201-9.

Vial C, Roberts JA and Evans RJ (2004) Molecular properties of ATP-gated P2X receptor ion channels. *Trends Pharmacol Sci* **25**:487-93.

Virginio C, MacKenzie A, Rassendren FA, North RA and Surprenant A (1999) Pore dilation of neuronal P2X receptor channels. *Nat Neurosci* **2**:315-21.

Molecular Pharmacology Fast Forward. Published on February 8, 2006 as DOI: 10.1124/mol.105.019802
This article has not been copyedited and formatted. The final version may differ from this version.

Footnotes - The nucleotide sequences for mouse $P2X_{2a}$, $P2X_{2b}$ and $P2X_{2e}$ have been deposited in the GenBank database under GenBank Accession Numbers AY044240, AB094664, and AB094663, respectively.

This study was supported by grants-in-aid from the Ministry of Education, Science, Sports, Culture and Technology of Japan (T.K., G.T.), the 21st Century COE program "Knowledge Information Infrastructure for Genome Science", by the Special Coordination Fund for Promoting Science and Technology (G.T.), and by the Intramural Research Program of the NICHD, NIH (K.K., M-L.H., S.S.S.).

Address correspondence and reprint requests to:
Gozoh Tsujimoto, M.D., Ph.D.
Department of Genomic Drug Discovery Science, Graduate School of Pharmaceutical Sciences, Kyoto University Faculty of Pharmaceutical Sciences, Kyoto University, Yoshida Shimoadachi-cho, Sakyo-ku, Kyoto 606-8501, Japan
Tel: ++81-75-753-4523, Fax: ++81-75-753-4544, E-mail: gtsuji@pharm.kyoto-u.ac.jp

Molecular Pharmacology Fast Forward. Published on February 8, 2006 as DOI: 10.1124/mol.105.019802
This article has not been copyedited and formatted. The final version may differ from this version.

FIGURE LEGENDS

Fig. 1. C-terminal structures and expression patterns of mouse $P2X_2$ isoforms. A, Schematic representation and cytoplasmic C-terminal sequences of mouse $P2X_2$ receptors. N and C represent amino- and carboxyl-termini, respectively. TM1 and TM2, first and second transmembrane domains, respectively. Sequences spliced out were shown as dashed lines. All splicing donor and acceptor sites follow GT/AG rule (underlined). The nucleotide base pairs (bp), starting at the initial AUG codon, were indicated at right. B, Expression of the $P2X_2$ receptor in mouse pituitary was examined by RT-PCR using a primer set that detects different C-terminal splicing patterns. Southern blotting and hybridization with a probe common to all $P2X_2$ isoforms detected three splicing variants. The expected lengths of the PCR products for $P2X_{2a}$, $P2X_{2b}$, and $P2X_{2e}$ were amplified from cDNAs as 686, 479, and 416 bp bands, respectively. RT+ and RT– indicate cDNAs prepared with and without the reverse transcriptase transcription step. C, Tissue-specific expression profiles of the $P2X_2$ isoforms were examined in: B, whole brain; Sp, spinal cord; H, heart; L, lung; K, kidney; Li, liver; Pa, pancreas; Ad, adrenal grand; M, neonatal cardiacmyocyte; and Fi, fibroblast. V, As a positive control mixture of cDNAs for $P2X_{2a}$, $P2X_{2b}$, and $P2X_{2e}$ was used; and water (W) as a negative control. D, Western blot analysis of $P2X_2$ isoforms. FLAG-tagged $P2X_2$ isoforms expressed in HEK cells were immunologically detected on the membrane. Kd, molecular weight markers.

Fig. 2. Patterns of 100 μM ATP-induced current profiles of $P2X_2$ receptors expressed in mammalian GT1 (left panels) and HEK cells (right panels). A-C, Representative traces of $P2X_{2a}$ (A), $P2X_{2b}$ (B) and $P2X_{2e}$ (C) currents during the prolonged application of ATP. Numbers below traces indicate the mean ± SEM values of rates of receptor desensitization. Single exponential functions were applied to describe the desensitization rates (τ_{des}). Numbers in parentheses indicate number of cells. *, $P < 0.05$ vs. $P2X_{2a}$; ** $P < 0.01$ vs. $P2X_{2b}$ receptor.

Fig. 3. Patterns of ATP-induced $[Ca^{2+}]_i$ profiles in GT1 cells expressing mouse $P2X_2$ isoform receptors. A-C, Dose-dependent activation and desensitization of homomeric $P2X_{2a}$ (A), $P2X_{2b}$ (B) and $P2X_{2e}$ receptors (C). In this and the following figures, experimental records are shown by circles (mean values from at least 15 traces in representative experiments) and fitted curves are shown by full lines. Single exponential functions were applied to describe the desensitization rates. Agonists were added to a final concentration, which is indicated above the traces and were

Molecular Pharmacology Fast Forward. Published on February 8, 2006 as DOI: 10.1124/mol.105.019802
This article has not been copyedited and formatted. The final version may differ from this version.

continuously present during the recording (horizontal bars). Dose-dependent peak $[Ca^{2+}]_i$ amplitudes (right, open circles) and desensitization rates (right, filled circles) were plotted against ATP concentrations. Dotted vertical lines indicate the calculated EC_{50} values.

Fig. 4. Functional expression of mouse $P2X_2$ isoforms in *Xenopus* oocytes. A, Schematic representations of C-terminal splicing and N-terminal deletion constructs. Three $P2X_2$ variants were deleted for 13 amino acids at their N-terminus (labeled as Δ1-13). B, Current kinetics of native and mutant $P2X_2$ receptors. ATP (100 μM) was applied for 30 s as indicated by the horizontal bars above traces. C, The decay phase of the current response was plotted against time after peak activation (mean ± SEM values, n = 7). Significant differences ($P < 0.05$) were observed between wild type (filled symbols) and N-terminally deleted (open symbols) subunit constructs of $P2X_{2a}$ (circles), $P2X_{2b}$ (squares) and $P2X_{2e}$ (triangles), respectively.

Fig. 5. Calcium signals in GT1 cells expressing native and mutant mouse P2X receptors. A-C, Wild type and N-terminally deleted $P2X_{2a}$ (A), $P2X_{2b}$ (B) and $P2X_{2e}$ (C) were expressed separately in GT1 cells and stimulated with 100 μM ATP. Left panels, representative traces of mean values from a single experiment performed simultaneously on 15 to 45 cells. Right panels, mean ± SEM values for calculated desensitization rates (left) and steady state $[Ca^{2+}]_i$ levels (right) are indicated, with a sample size of between 5 and 8 independent experiments. Desensitization level (%) scales indicate the percentage of decline in peak $[Ca^{2+}]_i$ response at 400 s of recording after subtracting basal $[Ca^{2+}]_i$ levels. *, $P < 0.05$, compared to subunits with intact N-termini. WT, $P2X_2$ isoforms having a full N-terminus. Mutant, N-terminal deletion mutants.

Fig. 6. Functional expression of N- or C-terminally tagged $P2X_2$ subunits. A, Dose-response curves were constructed using single GT1 cell $[Ca^{2+}]_i$ measurements and ATP as an agonist. Each point represents the mean ± SEM value from 15 – 33 traces collected from five experiments. B top, Intracellular localization of YFP-tagged subunits in HEK cells 48 hr after transient transfection detected by conforcal microscopy. White bar indicates 20 μm. B, bottom, Typical profiles of ATP (50 μM)-induced changes in $[Ca^{2+}]_i$ in GT1 cells expressing YFP-tagged $P2X_2$ subunits. C, Immunological detection of tagged $P2X_2$ subunit. GFP- or Luc-tagged subunits were detected as expected molecular weight. No additional splicing product was observed in cells expressing $P2X_{2a}$ and $P2X_{2b}$. D. Heteromer formation between differentially tagged $P2X_2$ subunits.

Molecular Pharmacology Fast Forward. Published on February 8, 2006 as DOI: 10.1124/mol.105.019802
This article has not been copyedited and formatted. The final version may differ from this version.

YFP-tagged $P2X_2$ subunits and Flag-$P2X_{2a}$-Luc constructs were examined for their co-immunoprecipitation. Cellular lysate was incubated with anti-Flag antibody and antigen-antibody complex was precipitated with protein G sepharose. Signals from YFP antibody were detected on a western blot membrane only from cells expressing both YFP- and Luc-tagged subunits. Kd, molecular weight markers. Representative figures from three independent experiments. E, Desensitization rates of N- or C-terminally tagged $P2X_2$ channels, estimated in GT1 cells by single cell $[Ca^{2+}]_i$ recordings. Data are from 18 – 26 cells. $P < 0.05$ vs. $P2X_{2a}$ constructs. F, Functional heteromultimer formation by YFP-tagged $P2X_2$ subunits. Chimeric $P2X_{2a}/X_3$ex subunit was expressed with $P2X_{2a}$-YFP or $P2X_{2e}$-YFP in GT1 cells and stimulated with 10 μM αβ-methylene ATP. Notice the difference in the rate of calcium signal decay. Homomeric $P2X_{2a}$ and $P2X_{2e}$ receptors were insensitive to 10 μM αβ-methylene (traces not shown). $P2X_{2a}/X_3$ex chimera represents a mutant subunit in which the extracellular regions from Ile^{66} to Tyr^{310} of rat $P2X_{2a}$ were replaced with Val^{60} to Phe^{300} of rat $P2X_3$.

Fig. 7. Homo-oligomer formation detected by luminescence spectra measurements. A, HEK cells co-expressing Luc and YFP constructs were collected in suspension and subjected to spectra measurement (n = 4). Bioluminescence was initiated by the addition of 5 μM coelenterazine h. Signal intensities at 480 nm and 535 nm were considered to arise from Luc and a combination of Luc and YFP, respectively. Asterisks indicate a significant increase in BRET ratio compared to that of Luc and YFP expressed cells ($P < 0.01$). B, BRET signal was stable in cells expressing different levels of tagged channels. 3.5 or 2 μg of cDNAs for YFP- and Luc-tagged $P2X_{2e}$ were co-transfected into HEK cells grown in 10 cm dishes and YFP fluorescence (bars, left axis) and BRET signals were measured (filled circles, right axis). Results were from three independent experiments. *, $P < 0.05$. C, Time course of BRET signals in response to 100 μM ATP application. Data presented were from single traces and similar results were observed in three independent experiments.

Fig. 8. C-terminal splicing enhances BRET efficiency between receptor C-termini. A, Either Luc or YFP was tagged at the C-terminal end of $P2X_2$ subunit and co-expressed in HEK cells (top panel). Bioluminescence from a suspension of cells was evoked by the addition of 5 μM coelenterazine h and spectra measurement was performed without excitation light. The light intensity was plotted against wavelength (three bottom panels). B, The wavelength for maximum

luminescence intensity detected from Luc was at 480 nm and for maximum fluorescence intensity from YFP fluorescence at 535 nm. The ratios of light intensities at 535/480 nm were compared and significant differences were observed in all combinations of $P2X_2$ variants (mean ± SEM values, n = 4).

Fig. 9. C-terminal splicing enhances BRET efficiency between subunits tagged at the N- and C-termini. A, BRET between C-terminal Luc and N-terminal GFP was examined (top panel). Light intensities detected were plotted against wavelength (three bottom panels). B, The wavelengths for peak intensities were at 480 nm for Luc and at 515 nm for GFP. The ratios of light intensities at 515/480 nm were compared and the significant differences were observed in all combinations of $P2X_2$ variants (mean ± SEM values, n = 4).

Fig. 10. Effects of deletion of amino acids from the $P2X_{2b}$ C-terminus results in conformational change. Two consecutive amino acids at the splicing junction, Val^{370} and Val^{371}, or at the C-terminal end, Gln^{402} and Leu^{403}, of $P2X_{2b}$ subunit were deleted and either Luc or YFP was connected to the C-terminal ends. BRET between C-terminal Luc and YFP of the mutant and original $P2X_{2b}$ receptors were examined in transfected HEK cells. A, Spectra measurements of cell suspensions. Intensities of light emitted from Luc and YFP were plotted against wavelength. B, The ratios of light intensities at 515/480 nm were compared and the significant differences are indicated by an asterisk ($P < 0.05$, n = 4-6). C, Desensitization rates of mutant and original $P2X_{2b}$ receptors were measured from single cell $[Ca^{2+}]_i$ changes induced by 100 μM ATP. Significant differences ($P < 0.05$) are indicated by an asterisk. Data presented were from six transfection experiments.

Fig. 11. A decrease of Flag-$P2X_{2a}$-Luc and $P2X_{2e}$-YFP heteromeric complex, but not Flag-$P2X_{2a}$-Luc and $P2X_{2a}$-YFP homomeric complex, after an increase in washing stringency of immunoprecipitated channels. A, Co-transfected subunits were immunoprecipitated with anti-Flag antibody as described in *Materials and Methods* and washed with increasing concentrations of NP40. Co-purified YFP-tagged $P2X_{2a}$ and $P2X_{2e}$ were detected on the western blot membrane. B, The amount of YFP-tagged $P2X_{2a}$ and $P2X_{2e}$ subunits were normalized with Flag-tagged $P2X_{2a}$-Luc. Results from three experiments were presented. *, $P < 0.05$ compared to the normalized band intensity of 0.5% NP40.

Figure 1

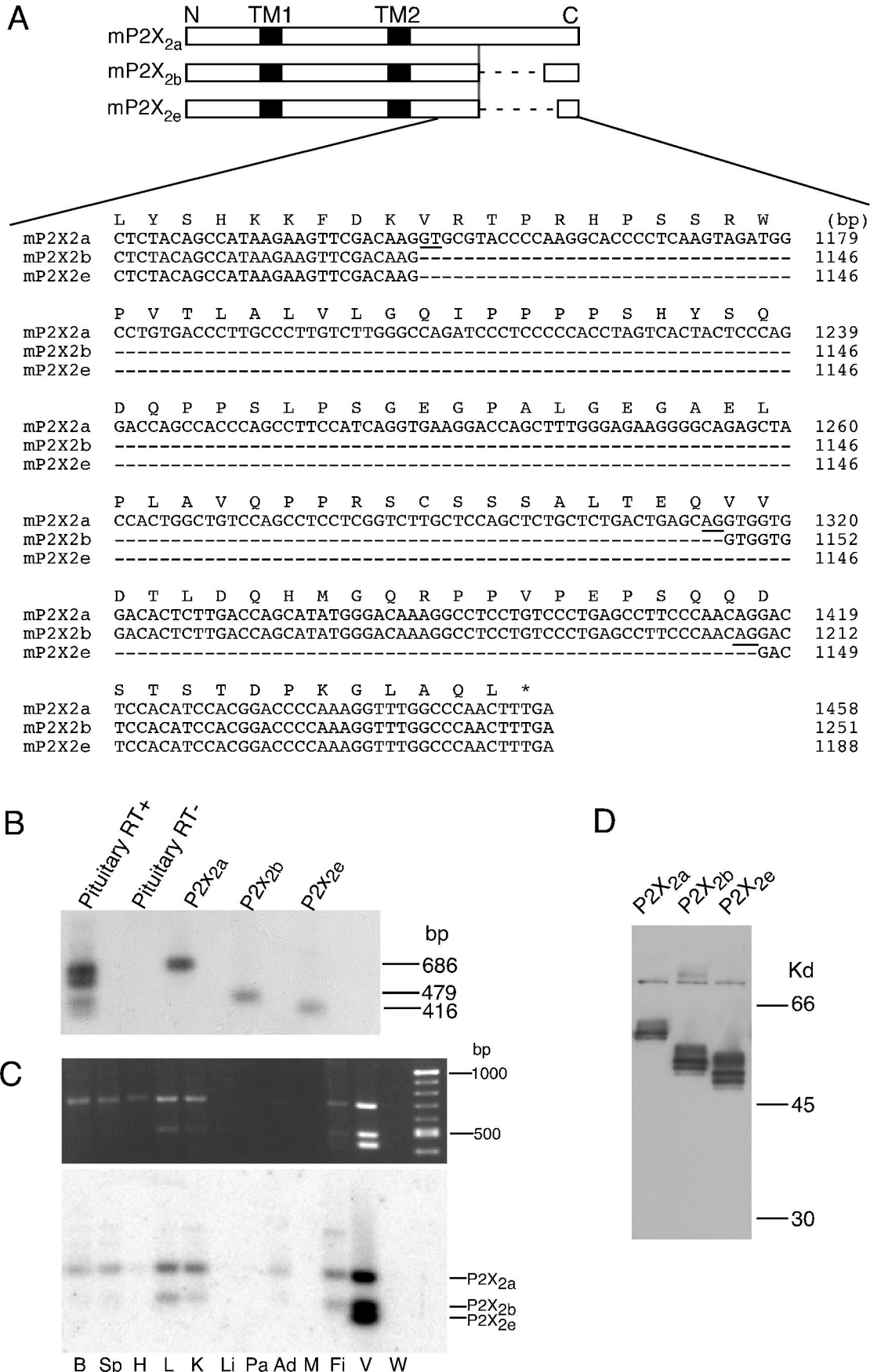
A
N
TM1
TM2
C
mP2X2a
mP2X2b
mP2X2e
L Y S H K K F D K V R T P R H P S S R W (bp)
mP2X2a CTCTACAGCCATAAGAAGTTCGACAAGGTGCGTACCCCAAGGCACCCCTCAAGTAGATGG 1179
mP2X2b CTCTACAGCCATAAGAAGTTCGACAAG---------- 1146
mP2X2e CTCTACAGCCATAAGAAGTTCGACAAG---------- 1146
P V T L A L V L G Q I P P P P S H Y S Q
mP2X2a CCTGTGACCCTTGCCCTTGTCTTGGGCCAGATCCCTCCCCCACCTAGTCACTACTCCCAG 1239
mP2X2b ---------- 1146
mP2X2e ---------- 1146
D Q P P S L P S G E G P A L G E G A E L
mP2X2a GACCAGCCACCCAGCCTTCCATCAGGTGAAGGACCAGCTTTGGGAGAAGGGGCAGAGCTA 1260
mP2X2b ---------- 1146
mP2X2e ---------- 1146
P L A V Q P P R S C S S S A L T E Q V V
mP2X2a CCACTGGCTGTCCAGCCTCCTCGGTCTTGCTCCAGCTCTGCTCTGACTGAGCAGGTGGTG 1320
mP2X2b ----------GTGGTG 1152
mP2X2e ---------- 1146
D T L D Q H M G Q R P P V P E P S Q Q D
mP2X2a GACACTCTTGACCAGCATATGGGACAAAGGCCTCCTGTCCCTGAGCCTTCCCAACAGGAC 1419
mP2X2b GACACTCTTGACCAGCATATGGGACAAAGGCCTCCTGTCCCTGAGCCTTCCCAACAGGAC 1212
mP2X2e ----------GAC 1149
S T S T D P K G L A Q L *
mP2X2a TCCACATCCACGGACCCCAAAGGTTTGGCCCAACTTTGA 1458
mP2X2b TCCACATCCACGGACCCCAAAGGTTTGGCCCAACTTTGA 1251
mP2X2e TCCACATCCACGGACCCCAAAGGTTTGGCCCAACTTTGA 1188
B
Pituitary RT+
Pituitary RT-
P2X2a
P2X2b
P2X2e
bp
686
479
416
C
bp
1000
500
P2X2a
P2X2b
P2X2e
B Sp H L K Li Pa Ad M Fi V W
D
P2X2a
P2X2b
P2X2e
Kd
66
45
30

Figure 2

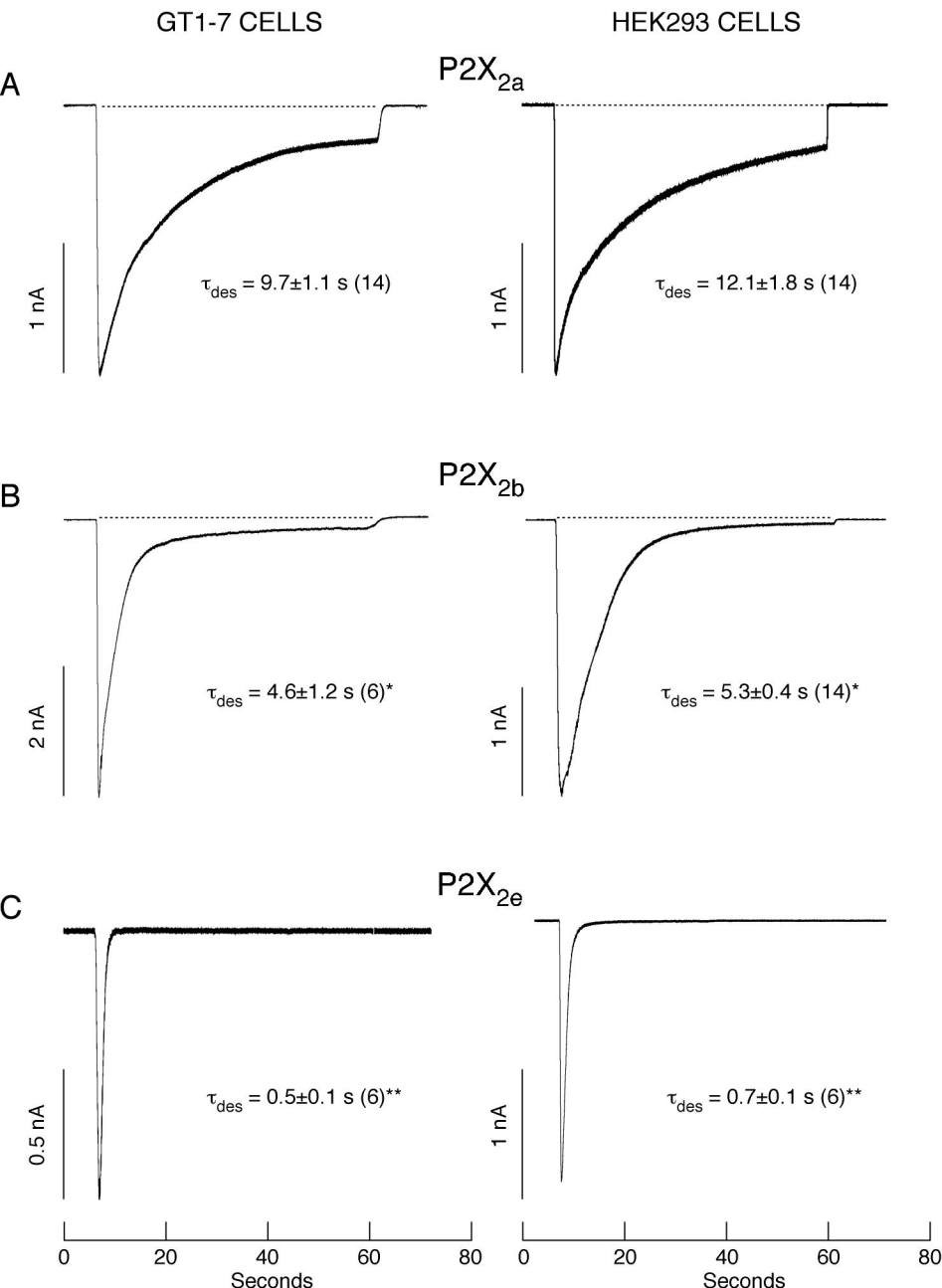
GT1-7 CELLS
HEK293 CELLS
A
P2X2a
1 nA
τdes = 9.7±1.1 s (14)
1 nA
τdes = 12.1±1.8 s (14)
B
P2X2b
2 nA
τdes = 4.6±1.2 s (6)*
1 nA
τdes = 5.3±0.4 s (14)*
C
P2X2e
0.5 nA
τdes = 0.5±0.1 s (6)**
1 nA
τdes = 0.7±0.1 s (6)**
0
20
40
60
80
Seconds
0
20
40
60
80
Seconds

Figure 3

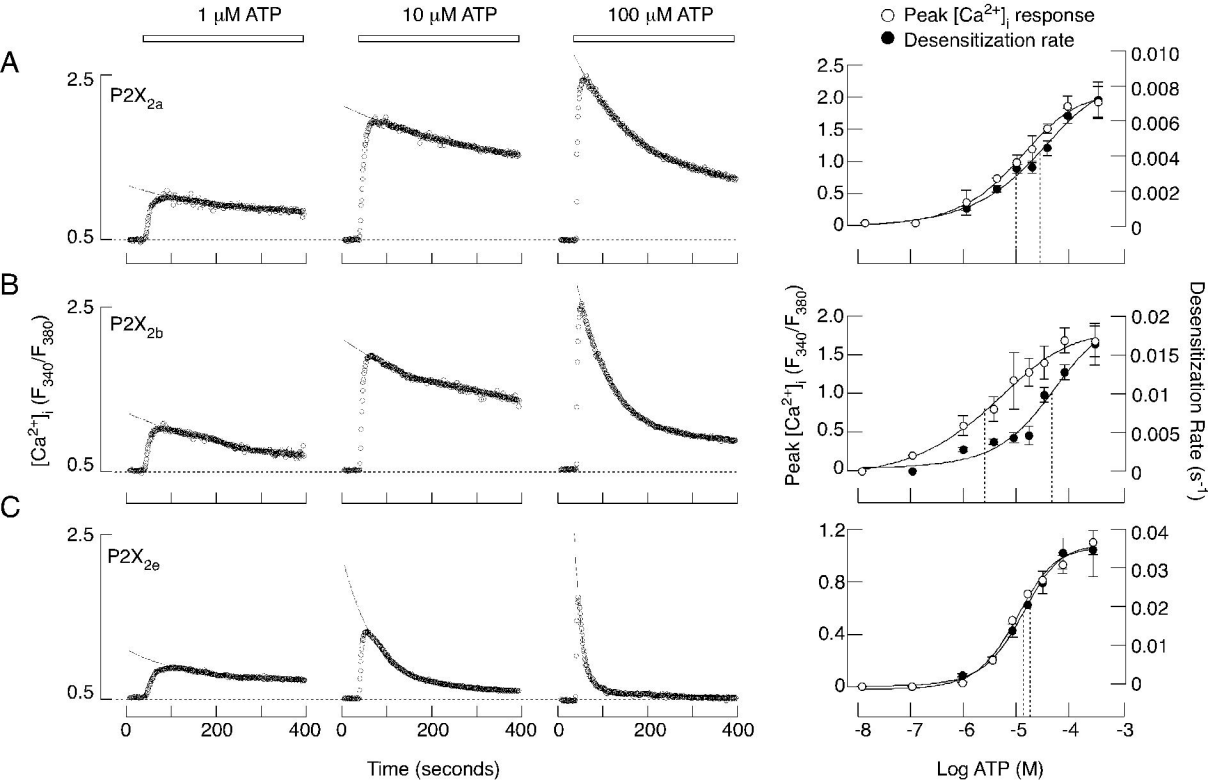
1 μM ATP
10 μM ATP
100 μM ATP
A
B
C
P2X2a
P2X2b
P2X2e
2.5
0.5
[Ca2+]i (F340/F380)
0
200
400
Time (seconds)
Peak [Ca2+]i response
Desensitization rate
Peak [Ca2+]i (F340/F380)
Desensitization Rate (s-1)
2.5
2.0
1.5
1.0
0.5
0
0.010
0.008
0.006
0.004
0.002
0.02
0.015
0.01
0.005
1.2
0.8
0.4
0.04
0.03
0.02
0.01
-8
-7
-6
-5
-4
-3
Log ATP (M)

Figure 4

A

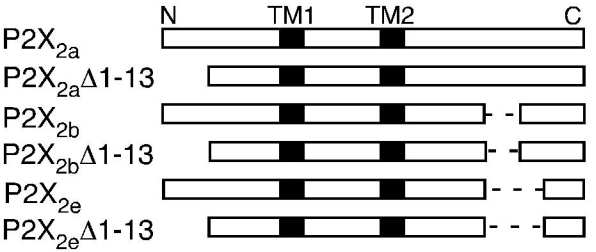
N
TM1
TM2
C
P2X2a
P2X2aΔ1-13
P2X2b
P2X2bΔ1-13
P2X2e
P2X2eΔ1-13

B

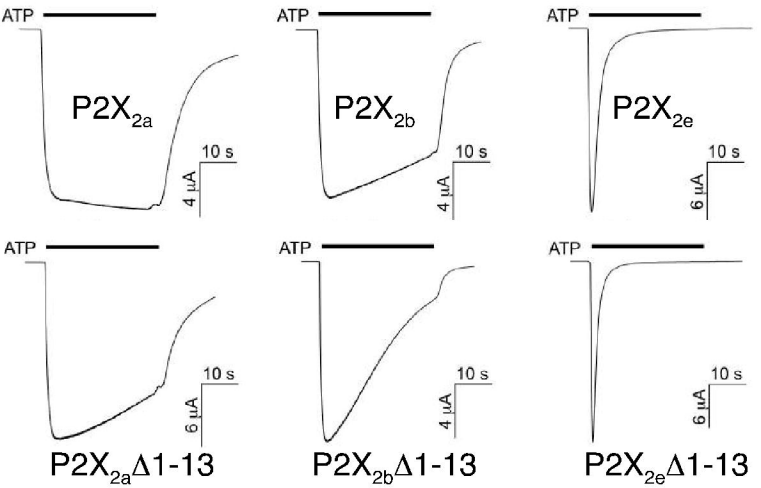
ATP
P2X2a
10 s
4 μA
ATP
P2X2b
10 s
4 μA
ATP
P2X2e
10 s
6 μA
ATP
10 s
6 μA
P2X2aΔ1-13
ATP
10 s
4 μA
P2X2bΔ1-13
ATP
10 s
6 μA
P2X2eΔ1-13

C

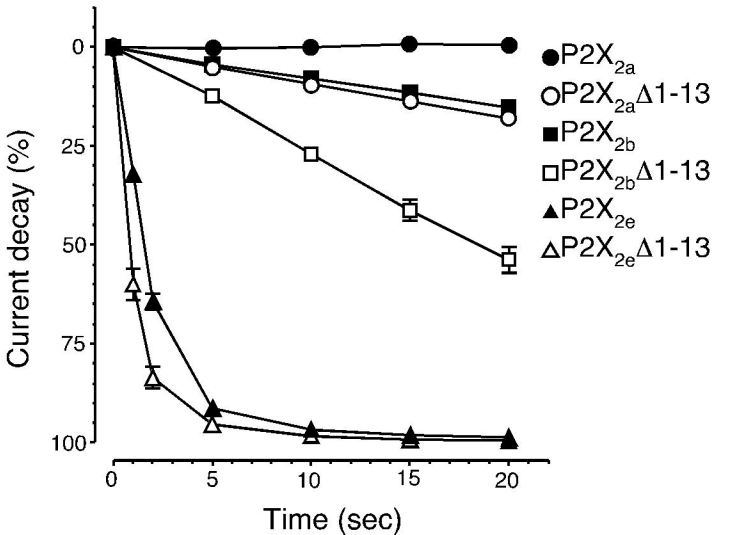
Current decay (%)
0
25
50
75
100
0
5
10
15
20
Time (sec)
P2X2a
P2X2aΔ1-13
P2X2b
P2X2bΔ1-13
P2X2e
P2X2eΔ1-13

Figure 5

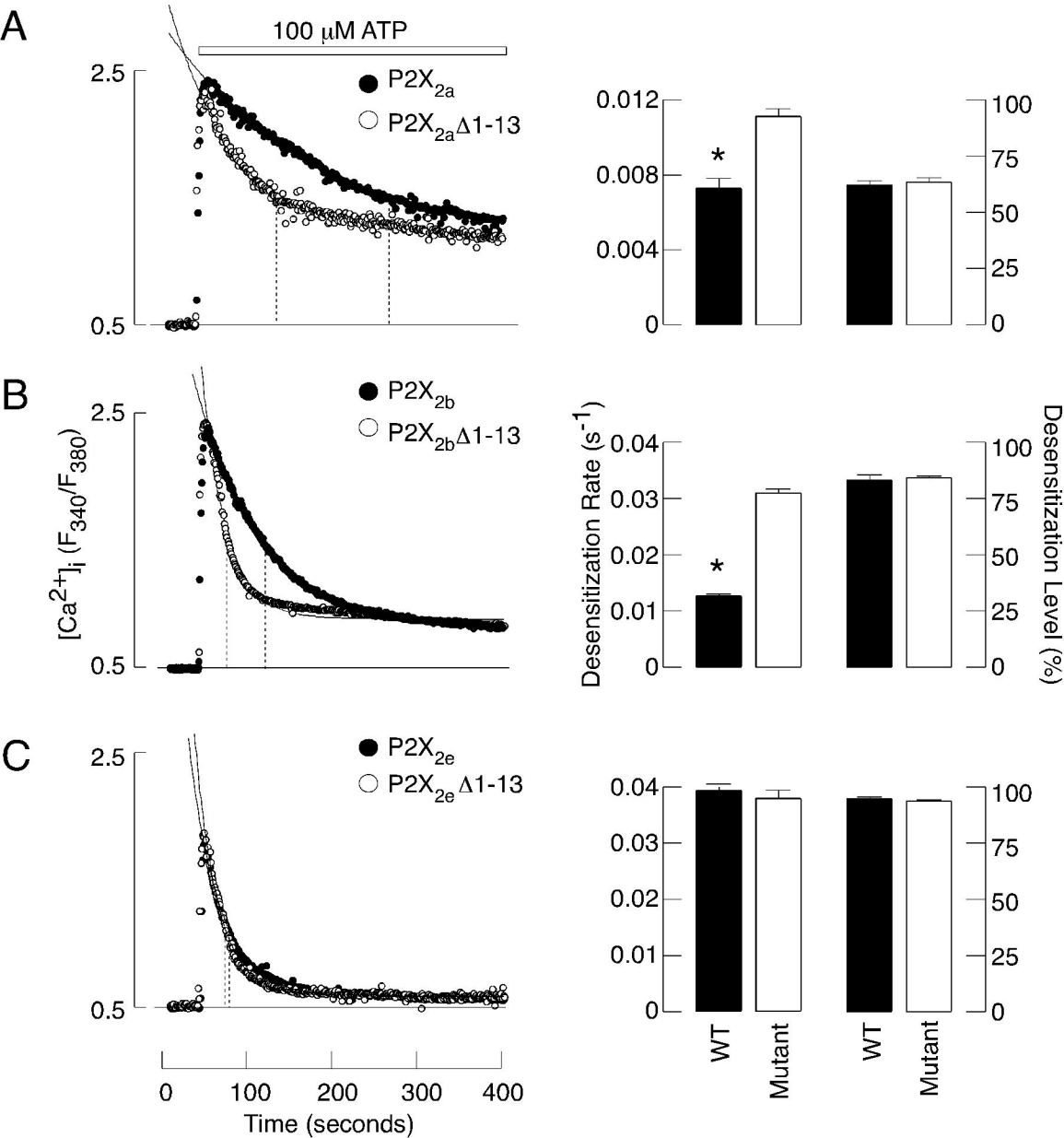
A
100 μM ATP
2.5
0.5
P2X2a
P2X2aΔ1-13
0.012
0.008
0.004
0
100
75
50
25
0
*
B
[Ca2+]i (F340/F380)
P2X2b
P2X2bΔ1-13
Desensitization Rate (s-1)
Desensitization Level (%)
0.04
0.03
0.02
0.01
*
C
P2X2e
P2X2eΔ1-13
0
100
200
300
400
Time (seconds)
WT
Mutant
WT
Mutant

Figure 6

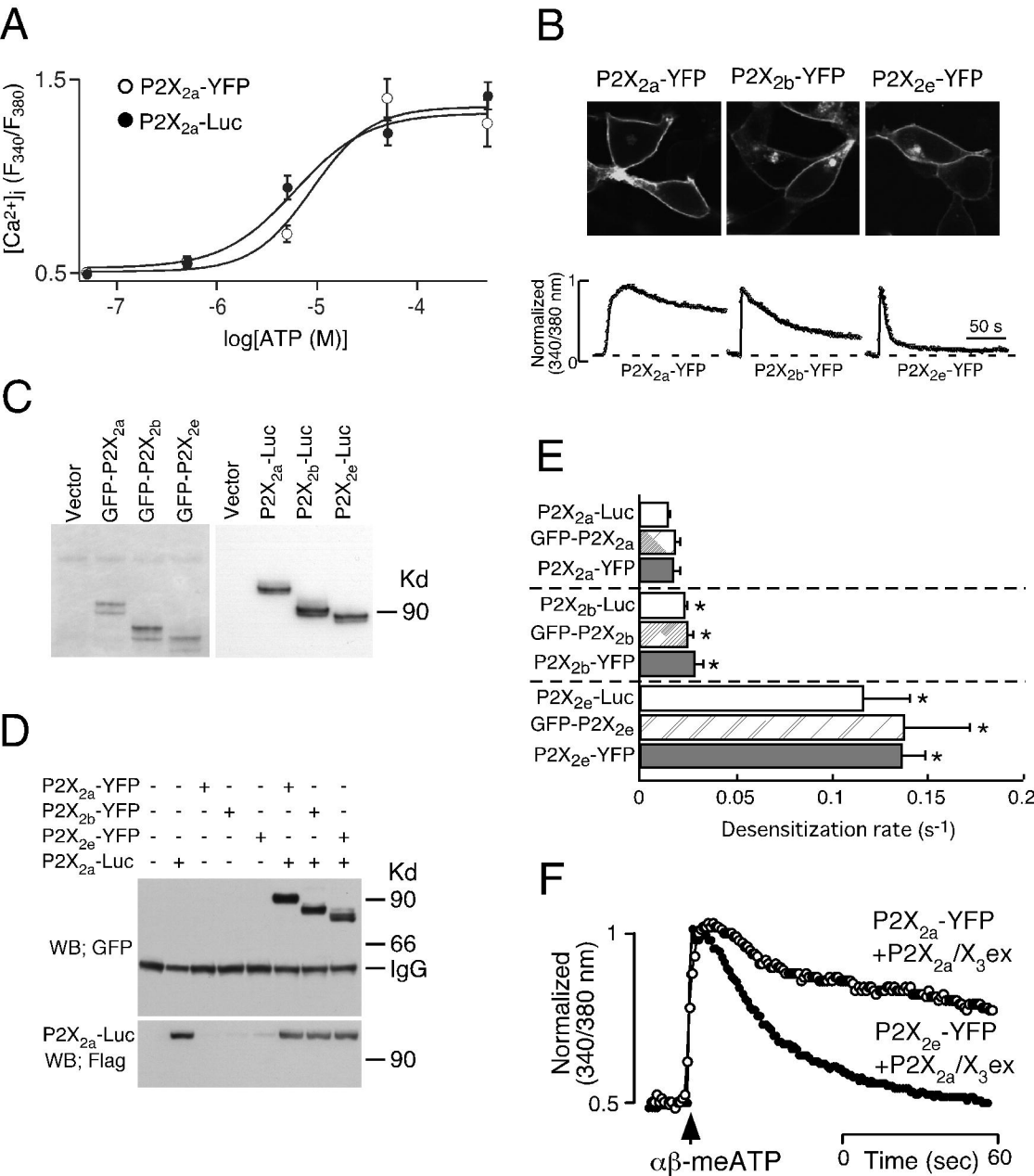
A
B
C
D
E
F
P2X2a-YFP
P2X2a-Luc
log[ATP (M)]
P2X2b-YFP
P2X2e-YFP
Normalized (340/380 nm)
50 s
Vector
GFP-P2X2a
GFP-P2X2b
GFP-P2X2e
P2X2a-Luc
P2X2b-Luc
P2X2e-Luc
Kd
90
WB; GFP
66
IgG
WB; Flag
GFP-P2X2a
P2X2a-YFP
GFP-P2X2b
P2X2b-YFP
GFP-P2X2e
P2X2e-YFP
Desensitization rate (s-1)
+P2X2a/X3ex
αβ-meATP
Time (sec)

Figure 7

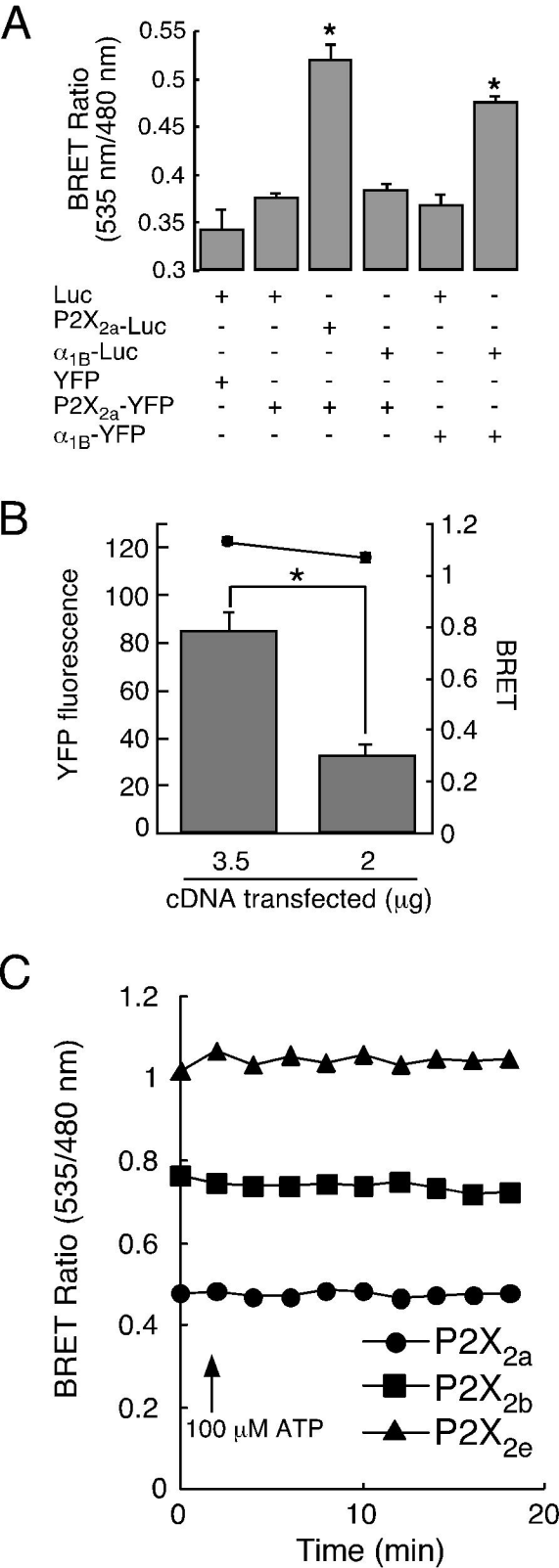
A
BRET Ratio (535 nm/480 nm)
0.55
0.5
0.45
0.4
0.35
0.3
*
*
Luc + + - - + -
P2X2a-Luc - - + - - -
α1B-Luc - - - + - +
YFP + - - - - -
P2X2a-YFP - + + + - -
α1B-YFP - - - - + +
B
YFP fluorescence
120
100
80
60
40
20
0
BRET
1.2
1
0.8
0.6
0.4
0.2
0
*
3.5
2
cDNA transfected (μg)
C
BRET Ratio (535/480 nm)
1.2
1
0.8
0.6
0.4
0.2
0
100 μM ATP
P2X2a
P2X2b
P2X2e
0
10
20
Time (min)

Figure 8

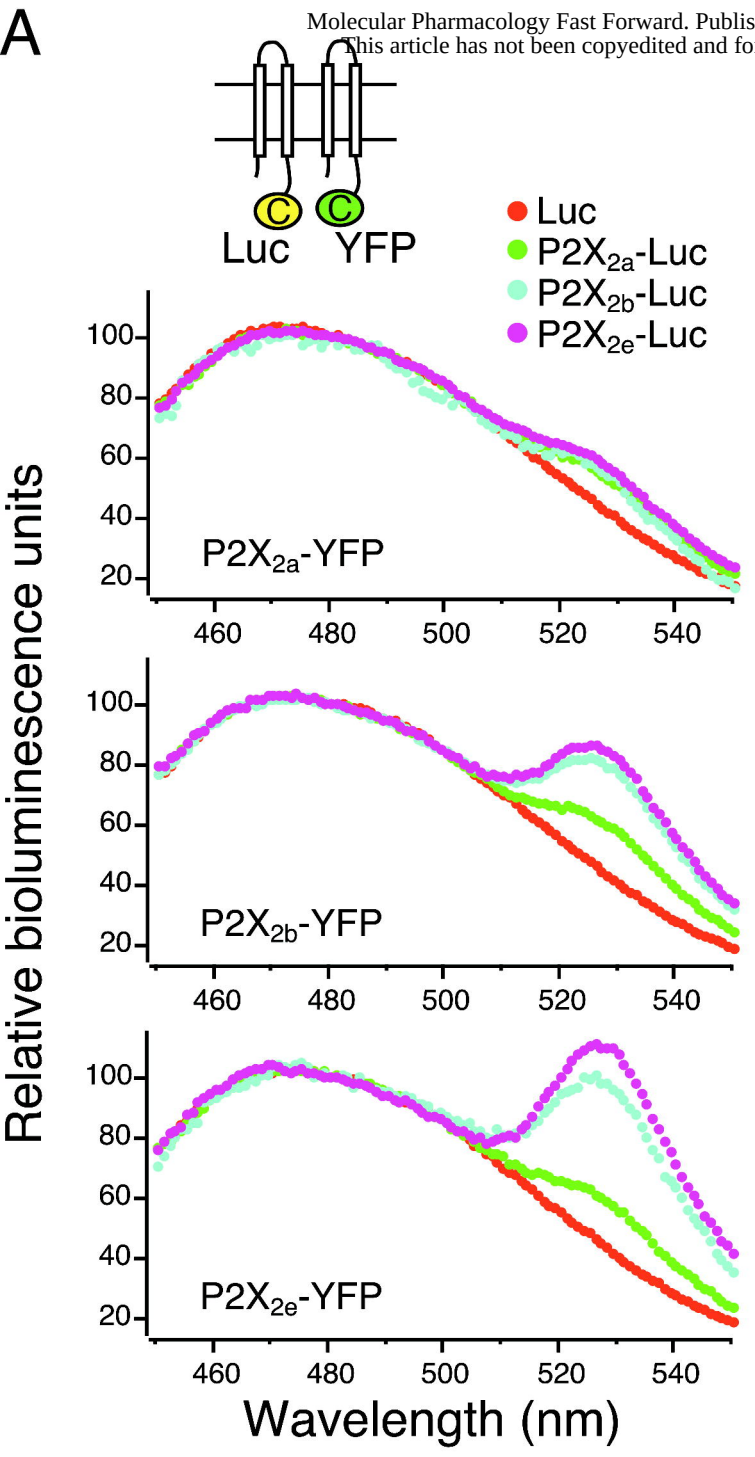

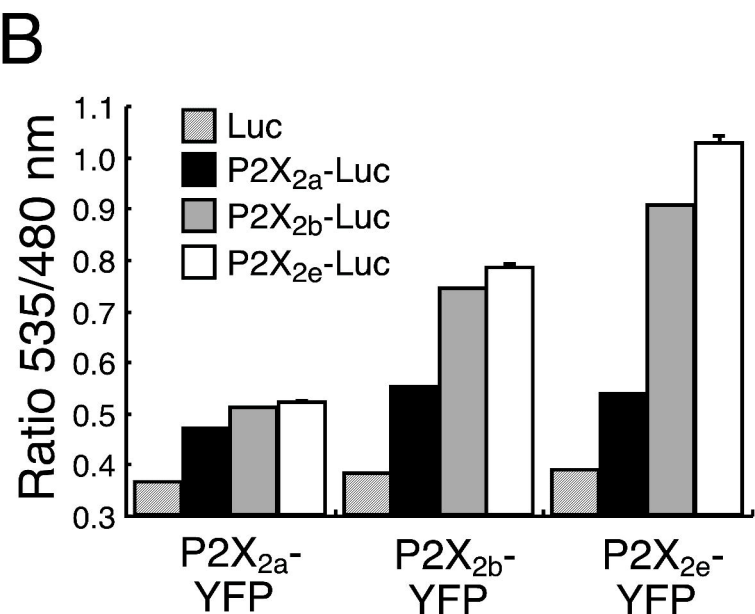

Figure 9

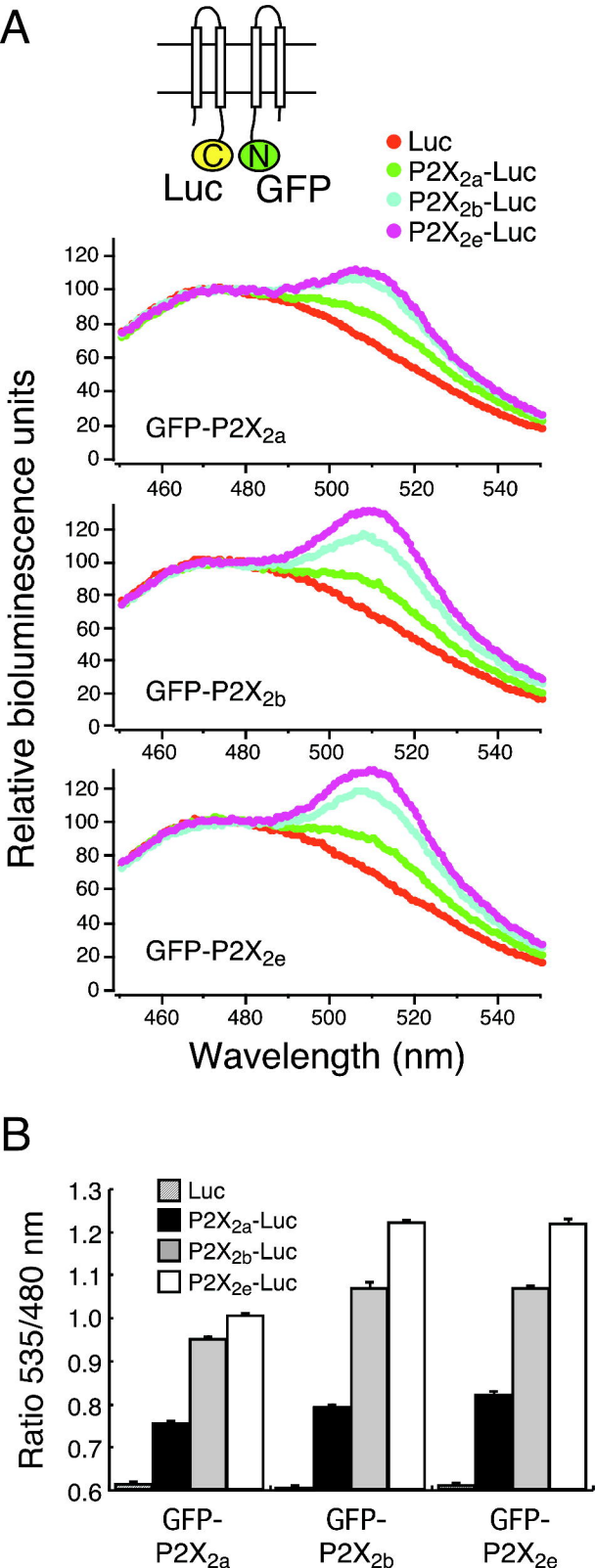
A
C
N
Luc
GFP
Luc
P2X2a-Luc
P2X2b-Luc
P2X2e-Luc
Relative bioluminescence units
GFP-P2X2a
GFP-P2X2b
GFP-P2X2e
Wavelength (nm)
B
Ratio 535/480 nm
Luc
P2X2a-Luc
P2X2b-Luc
P2X2e-Luc
GFP-P2X2a
GFP-P2X2b
GFP-P2X2e

Figure 10

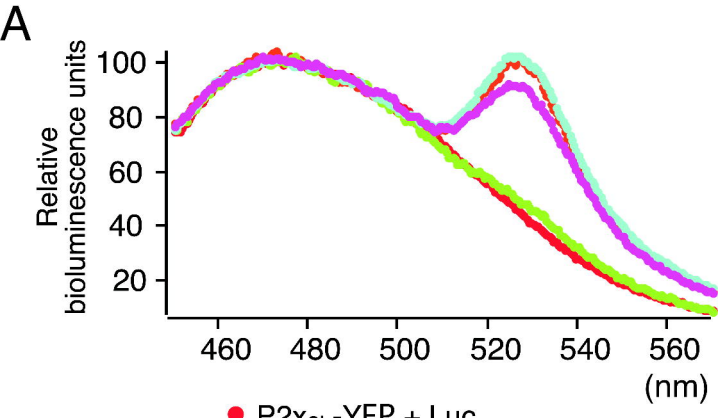
A
Relative bioluminescence units
100
80
60
40
20
460
480
500
520
540
560
(nm)
P2x2b-YFP + Luc
P2x2b-YFP + P2x2b-Luc
YFP + P2x2b-Luc
P2x2b-Δ402-403-YFP + P2x2b-Δ402-403-Luc
P2x2b-Δ370-371-YFP + P2x2b-Δ370-371-Luc

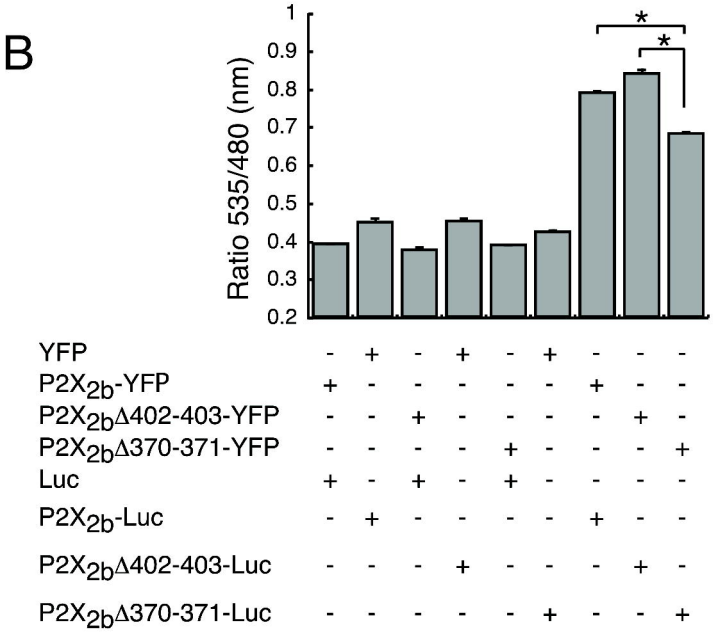
B
Ratio 535/480 (nm)
1
0.9
0.8
0.7
0.6
0.5
0.4
0.3
0.2
*
*
YFP - + - + - + - - -
P2X2b-YFP + - - - - - + - -
P2X2bΔ402-403-YFP - - + - - - - + -
P2X2bΔ370-371-YFP - - - - + - - - +
Luc + - + - + - - - -
P2X2b-Luc - + - - - - + - -
P2X2bΔ402-403-Luc - - - + - - - + -
P2X2bΔ370-371-Luc - - - - - + - - +

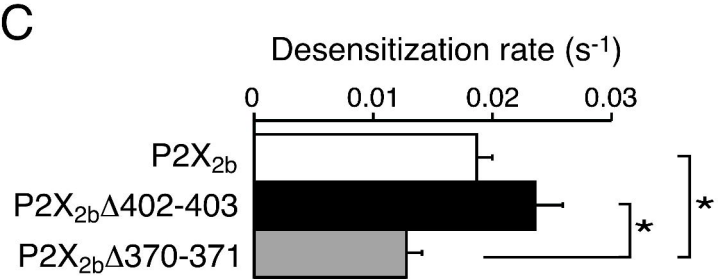
C
Desensitization rate (s-1)
0
0.01
0.02
0.03
P2X2b
P2X2bΔ402-403
P2X2bΔ370-371
*
*

Figure 11

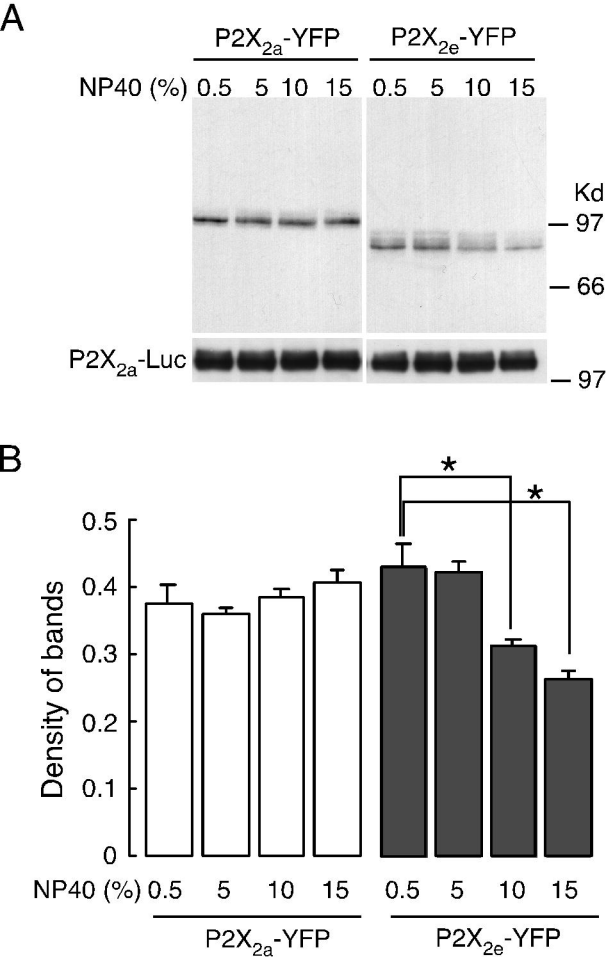
A
P2X2a-YFP
P2X2e-YFP
NP40 (%) 0.5 5 10 15 0.5 5 10 15
Kd
97
66
P2X2a-Luc
97
B
*
*
Density of bands
0.5
0.4
0.3
0.2
0.1
0
NP40 (%) 0.5 5 10 15 0.5 5 10 15
P2X2a-YFP
P2X2e-YFP